

## Article

# Theoretical Impact of Building Façade Thickness on Daylight Metrics and Lighting Energy Demand in Buildings: A Case Study of the Tropics

Rizki A. Mangkuto <sup>1</sup>, Atthailah <sup>2,3,\*</sup> , Mochamad Donny Koerniawan <sup>4</sup>  and Brian Yulianto <sup>5</sup> 

<sup>1</sup> Building Physics Research Group, Faculty of Industrial Technology, Institut Teknologi Bandung, Jl. Ganesha 10, Labtek VI, Bandung 40132, Indonesia; armanto@tf.itb.ac.id

<sup>2</sup> Engineering Physics Doctorate Program, Faculty of Industrial Technology, Institut Teknologi Bandung, Jl. Ganesha 10, Labtek VI, Bandung 40132, Indonesia

<sup>3</sup> Architecture Program, Faculty of Engineering, Universitas Malikussaleh, Jl. Cot Teungku Nie, Aceh Utara 24355, Indonesia

<sup>4</sup> Building Technology Research Group, School of Architecture, Planning, and Policy Development, Institut Teknologi Bandung, Jl. Ganesha 10, Labtek IXB, Bandung 40132, Indonesia; donny@ar.itb.ac.id

<sup>5</sup> Advanced Functional Material Research Group, Faculty of Industrial Technology, Institut Teknologi Bandung, Jl. Ganesha 10, Labtek VI, Bandung 40132, Indonesia; brian@tf.itb.ac.id

\* Correspondence: atthailah@unimal.ac.id

**Abstract:** In daylighting design, variation of building façade thickness ( $f$ ) will result in variation of the daylight opening areas, which in turn will modify the values of daylight metrics within the space. However, studies dedicated to investigating the impact of varying  $f$  on indoor daylight metrics are relatively scarce. This study, therefore, aims to assess the theoretical impact of various façade thicknesses on various daylight metrics and lighting energy demands in a reference office space. Analytical calculations are performed using an outdoor diffuse illuminance profile of a tropical city. The building façade thickness values are varied within 0–0.50 m, at window-to-wall ratios (WWR) of 25%, 50%, and 75%. Based on sensitivity analysis, it is found that variation of  $f$  yields different impacts on the observed metrics, with  $sDA_{300/50\%}$  being the least influenced. Among all metrics in the central calculation point,  $DA_{300}$ ,  $UDI-a$ , and  $UDI-a'$  yield relatively small coefficients of variation, and thus, have the lowest uncertainty with respect to  $f$ . Among all metrics for the entire room,  $sDA_{300/50\%}$  and  $sUDI-a_{50\%}$  have the lowest uncertainty, with interquartile ranges of no more than 0.4%. Overall, the contribution of this study is providing insight into the impact of façade thickness on various daylight metrics in indoor spaces, particularly in the worst-case scenario under the standard CIE overcast sky.

**Keywords:** daylighting; façade thickness; overcast sky; daylight metrics; lighting energy demand



**Citation:** Mangkuto, R.A.; Atthailah; Koerniawan, M.D.; Yulianto, B. Theoretical Impact of Building Façade Thickness on Daylight Metrics and Lighting Energy Demand in Buildings: A Case Study of the Tropics. *Buildings* **2021**, *11*, 656. <https://doi.org/10.3390/buildings11120656>

Academic Editor: Isaac Guedi Capeluto

Received: 23 November 2021

Accepted: 14 December 2021

Published: 17 December 2021

**Publisher's Note:** MDPI stays neutral with regard to jurisdictional claims in published maps and institutional affiliations.



**Copyright:** © 2021 by the authors. Licensee MDPI, Basel, Switzerland. This article is an open access article distributed under the terms and conditions of the Creative Commons Attribution (CC BY) license (<https://creativecommons.org/licenses/by/4.0/>).

## 1. Introduction

Over the past two or three decades, there has been a large body of research highlighting the physical, physiological, and/or psychological benefits of daylight admission in buildings. It is also widely understood that daylight can improve the building occupants' performance and health (e.g., [1–7]). An excessive daylight admission may, however, increase the risk of visual and thermal discomfort, as well as the total building energy demand (e.g., [8–12]), so that careful considerations in the design phase are required.

The current practice of daylighting design in buildings typically employs computational modelling and simulation so that the impact of the proposed design parameters on the indoor environmental quality can be better predicted. Among many relevant design parameters, the opening area or window-to-wall ratio (WWR) is arguably the one most discussed due to the potential conflict that may arise between the resulting thermal, energy, and lighting performances of the indoor space (e.g., [11,13–17]).

Another daylighting design parameter that may reasonably influence the building performance is the façade or opening wall thickness. With respect to the thermal performance, it is obvious that the change (or uncertainty) of the façade's thickness will vary the thermal transmittance, the overall thermal transfer value, and the associated cooling or heating energy demand. This has been well reflected in the literature (e.g., [18–24]).

Meanwhile, with respect to (day) lighting performance, the change of façade thickness will change the effective daylight opening areas, which will also change the daylight metrics values within the space. However, studies dedicated to investigating the impact of varying façade thickness on indoor daylight metrics are relatively scarce. Several studies involving the so-called reference office space assume a certain baseline value for the façade thickness, for instance, 0.355 [25] or 0.150 m [26]. In the former study, possible variations between 0.295 and 0.325 m were proposed for the façade thickness, although they were observed only regarding the thermal performance. In the latter, no variations of thickness were considered. Indeed, the choice of façade thickness in actual constructions is determined by various technical considerations and regulations. However, since the consideration is mostly based on thermal performance requirements, an inexperienced designer may incorrectly think that the thickness has little to no influence on the daylighting performance. Nevertheless, further verification is still required on this matter.

A recent study [27] has investigated the impact of varying façade thickness on various daylight metrics and lighting energy demands by means of annual daylighting simulation, using the climate data of an Indonesian city. The study suggests that the average daylight factor ( $DF_{av}$ ) on the workplane is the metric that is the most influenced by façade thickness variation. However, the results are based on a constant WWR value, i.e., 25%, and thus may not be generalised for other values.

Moreover, the use of a more general approach, for instance, by considering the standard CIE overcast sky [28], is still needed to provide the idea of a 'worst-case' scenario. In fact, many national and regional standards (e.g., the former British standard BS 8206-2:2008 [29] and the recent EN 17037 [30]) still adopt(ed) the standard CIE overcast sky, which is implicitly indicated through the utilisation of daylight factor (DF) as one of the daylighting performance indicators.

The current study, therefore, aims to assess the theoretical impact of various façade thicknesses, which also includes an incorrect assumption of the values on various daylight metrics and lighting energy demands in a reference office space. The assessments are carried by means of analytical calculation, followed by sensitivity and uncertainty analyses, assuming the presence of the standard CIE overcast sky for the case of a tropical city.

The article is structured as follows. Sections 2 and 3, respectively, describe the relevant theoretical concept and the assessment method. Sections 4 and 5 provide the results and discussion, while Section 6 concludes the article.

## 2. Concept

### 2.1. Sky Component

To observe the worst-case scenario in daylighting design, the well-known standard CIE overcast sky is still in use to date, particularly to predict the daylighting performance under only diffuse daylight illuminance, regardless of the climate type and orientation. Under this sky model, the sky luminance  $L_\theta$  at a given elevation angle  $\theta$  (where  $0 \leq \theta \leq \pi/2$ ) and at any azimuth angle  $\psi$  reads:

$$L_\theta = L_z \frac{1 + 2 \sin \theta}{3} \quad (1)$$

where  $L_z$  is the zenith luminance.

It can be shown [31–33] that the horizontal illuminance  $E_{out}$  at any point on an unobstructed ground plane under this sky model reads:

$$E_{out} = \int_0^{2\pi} \int_0^{\pi/2} \frac{L_z}{3} (1 + 2 \sin \theta) \sin \theta \cos \theta \, d\theta \, d\psi = \frac{7}{9} \pi L_z \quad (2)$$

Consider now a black room with a vertical, rectangular daylight opening with length  $L$  and height  $H$  on one of the room walls (Figure 1), under the CIE standard overcast sky. Suppose inside the room there is a calculation point  $P$  on the horizontal (work) plane, at a distance  $D$  from the opening wall. The projection of  $P$  on the  $y$ - $z$  plane, where the opening sits, coincides with one of the vertices of the opening, which in this case is the lower-left vertex (Figure 1).

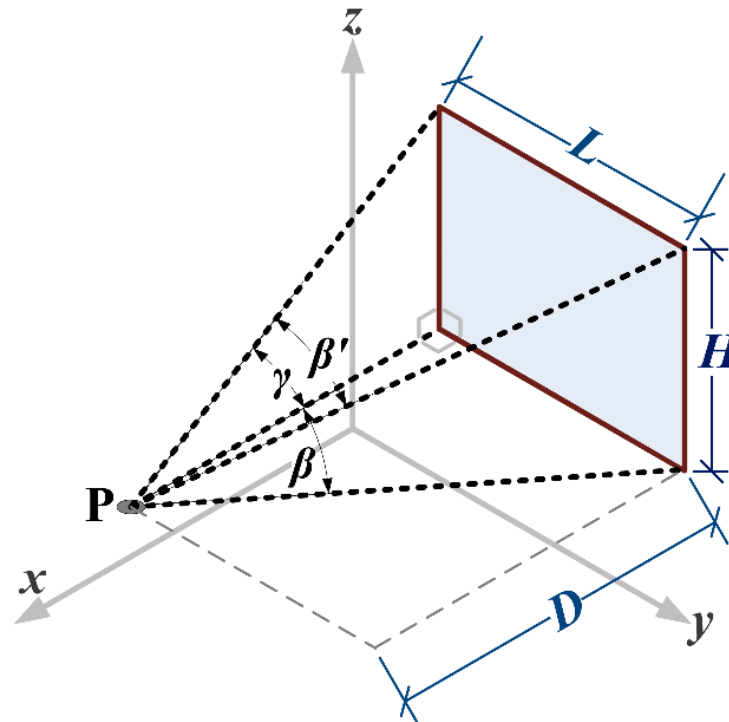


**Figure 1.** Isometric view of a calculation point  $P$  on the horizontal plane, at a distance  $D$  from a vertical, rectangular, effective daylight opening with length  $L$  and height  $H$ . The projection of  $P$  on the  $y$ - $z$  plane, where the opening sits, coincides with the lower-left vertex of the opening.

The ratio between  $E_{in,sky}$  and  $E_{out}$  is known as the sky component (SC) at the calculation point. The SC is of general interest because it is a purely geometrical variable, and its value shall remain the same so long as the geometrical configuration is unchanged. In the case of the configuration in Figure 1, it can be shown that the SC at  $P$  reads:

$$SC_P = \frac{E_{in,sky,P}}{E_{out}} = \frac{3}{14\pi}(\beta - \beta' \cos \gamma) + \frac{2}{7\pi} \arcsin(\sin \beta \sin \gamma) - \frac{1}{7\pi}(\sin 2\gamma \sin \beta') \quad (3)$$

Notice that the SC at  $P$ , in that case, depends only on the values of  $L$  and  $H$ , which represent the length and height of the effective opening, and obviously  $D$ , which is the distance. For practical reasons, one may write  $SC_P = SC(L, H)$  to indicate the dependency.

In the case where the façade thickness is non-zero, the effective daylight opening is smaller than that in the case with zero façade thickness, even in the absence of external obstructions and shading devices. To illustrate this, consider a vertical, rectangular daylight opening of actual length  $L_0$  and actual height  $H_0$  inside a black room, which has an internal height  $H_r$ , an internal width  $W_r$ , and a façade thickness  $f$ . For simplicity, the position of the opening is centred symmetrically on the façade. The lowest part of the actual opening is located at height  $z = z_{o1}$ , while the highest is at  $z = z_{o2}$ .

Suppose the calculation point  $P$  lies on the coordinate  $(x_P, y_P, z_P)$ , referring to Figure 1, in which  $x_P = D$  and  $z_P$  are taken as 0.75 m. Depending on  $x_P$  and  $y_P$ , there are four possible configurations in which  $SC_P$  can be calculated (Figures 2 and 3). These are as follows:

- (1)  $z_P \leq z_o$  and  $y_P \leq y_o$  (plan view: Figure 2a, section view: Figure 2c, elevation view: Figure 3a).
- (2)  $z_P \leq z_o$  and  $y_P > y_o$  (plan view: Figure 2a, section view: Figure 2d, elevation view: Figure 3b).
- (3)  $z_P > z_o$  and  $y_P \leq y_o$  (plan view: Figure 2b, section view: Figure 2c, elevation view: Figure 3c).
- (4)  $z_P > z_o$  and  $y_P > y_o$  (plan view: Figure 2b, section view: Figure 2d, elevation view: Figure 3d).

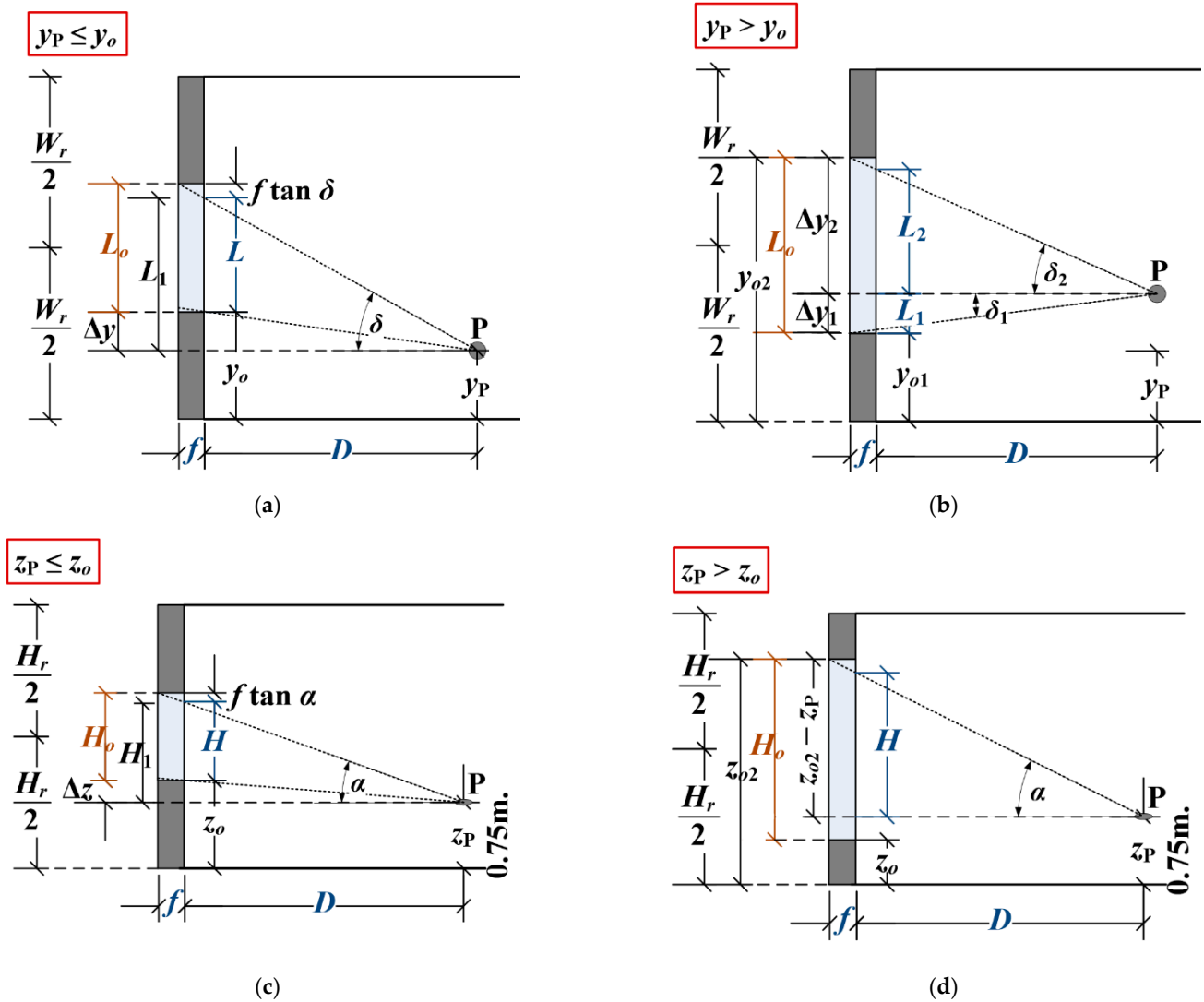


**Figure 2.** Plan view of the configuration in which (a)  $z_P \leq z_o$ , (b)  $z_P > z_o$ ; section view of the configuration in which (c)  $y_P \leq y_o$ , (d)  $y_P > y_o$ .

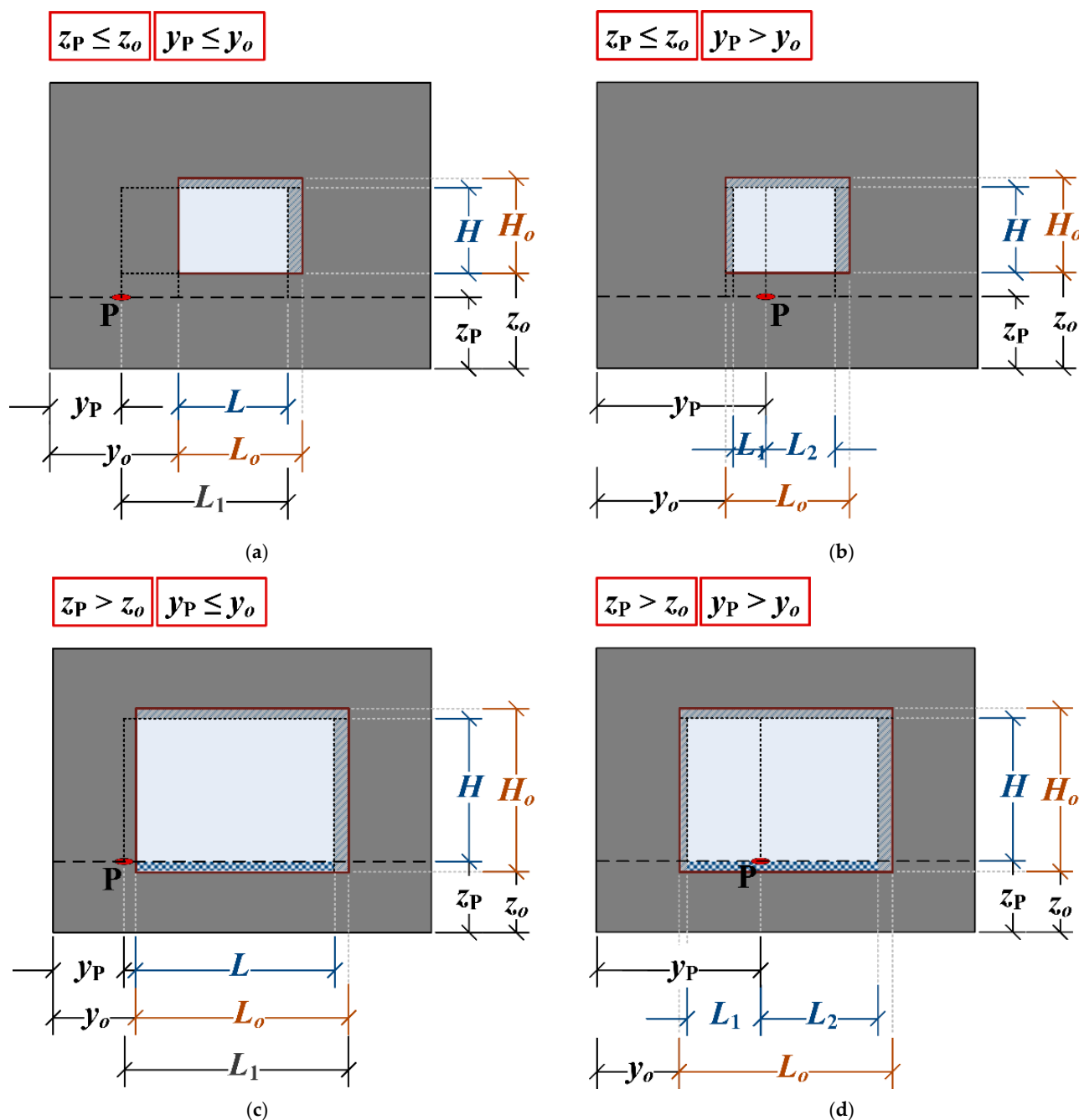


**Figure 3.** Elevation views of the configuration in which (a)  $z_P \leq z_o$  and  $y_P \leq y_o$ , (b)  $z_P \leq z_o$  and  $y_P > y_o$ , (c)  $z_P > z_o$  and  $y_P \leq y_o$ , (d)  $z_P > z_o$  and  $y_P > y_o$ .

The effective daylight opening in all configurations has the length  $L$  and height  $H$ , both of which are, respectively, smaller than  $L_o$  and  $H_o$ . In Figure 3, the effective daylight opening is shown by the unshaded areas. Notice that, despite the actual opening being symmetrically placed at the façade, the effective opening is, in general, not centred, unless  $P$  lies on the room's longitudinal axis (i.e.,  $y_P = W_r/2$ ).

In configuration (1), cf. Figure 3a, the SC at  $P$  reads:

$$SC_P = SC(L_1, H_1) - SC(\Delta y, H_1) + SC(\Delta y, \Delta z) - SC(L_1, \Delta y) \quad (4)$$

with reference to the text explaining Equation (3). From Figure 2a,c,  $L_1$  and  $H_1$  read:

$$L_1 = D \tan \delta = D \cdot \frac{L_0 + \Delta y}{D + f} = D \cdot \frac{L_0 + y_0 - y_P}{D + f} \quad (5)$$

$$H_1 = D \tan \alpha = D \cdot \frac{H_0 + \Delta z}{D + f} = D \cdot \frac{L_0 + z_0 - z_P}{D + f} \quad (6)$$

In configuration (2), cf. Figure 3b, the SC at P reads:

$$SC_P = SC(L_1, H_1) - SC(L_1, \Delta z) + SC(L_2, H_1) - SC(L_2, \Delta z) \quad (7)$$

From Figure 2d,  $L_1$  and  $L_2$  read:

$$L_1 = D \tan \delta_1 = D \cdot \frac{\Delta y_1}{D + f} = D \cdot \frac{y_P - y_0}{D + f} \quad (8)$$

$$L_2 = D \tan \delta_2 = D \cdot \frac{\Delta y_2}{D + f} = D \cdot \frac{y_0 - y_P}{D + f} \quad (9)$$

while  $H_1$  is as per Equation (11).

In configuration (3), cf. Figure 3c, the SC at P reads:

$$SC_P = SC(L_1, H) - SC(\Delta y, H) \quad (10)$$

where  $\Delta y = y_0 - y_P$ . Notice that the part of the opening that lies beneath the workplane, i.e.,  $z < z_P$ , is neglected from the SC calculation. From Figure 2b,  $H$  reads:

$$H = D \tan \alpha = D \cdot \frac{z_0 - z_P}{D + f} \quad (11)$$

while  $L_1$  is as per Equation (10).

In configuration (4), cf. Figure 3d, the SC at P reads:

$$SC_P = SC(L_1, H) + SC(L_2, H) \quad (12)$$

where  $L_1$  and  $L_2$  are as per Equations (8) and (9), while  $H$  is as per Equation (11).

## 2.2. Externally Reflected Component

Suppose now there are also reflections from the exterior surfaces that contribute to the horizontal illuminance value at the calculation point P. The so-called externally reflected component (ERC) at P is thus defined as the ratio between the illuminance contribution from the external reflections and  $E_{out}$ . Alternatively, ERC can be thought as the SC at P if the external obstructions are not present ( $SC_{obs}$ ), multiplied with the obstructions' reflectance ( $\rho_{obs}$ ), so that:

$$ERC_P = \rho_{obs} \cdot SC_{obs,P} \quad (13)$$

In the ideal case of a room with zero façade thickness and in the absence of external obstructions and shading devices, the ERC at any point inside the room is zero. However, in the case of non-zero façade thickness, the thick parts of the façade (which are outside the internal space of the room) shall obstruct the direct view to the sky from the calculation point, thus effectively reducing the daylight opening area. Nonetheless, the thick parts may also assume certain reflectance values, which eventually contribute to the internal illuminance, so that the ERC exists.

With reference to the four possible configurations in Section 2.1, the ERC at P can be determined by evaluating the  $SC_P$  from the grey-shaded opening areas in Figure 3, multiplied with the assumed reflectance value  $\rho_{obs}$ . If  $\rho_{obs}$  is assumed constant for the entire thick part of the façade, then in configuration (1), cf. Figure 3a, the ERC at P reads (prior to simplification):

$$SC_P = \rho_{\text{obs}} \{ SC(L_o + \Delta y, H_o + \Delta z) - SC(\Delta y, H_o + \Delta z) + SC(\Delta y, \Delta z) - SC(L_o + \Delta y, \Delta z) + SC(L_o + \Delta y, H_1) - SC(L_1, H_1) + SC(\Delta y, \Delta z) - SC(L_o + \Delta y, \Delta z) \} \quad (14)$$

In configuration (2), cf. Figure 3b, the ERC at P reads:

$$SC_P = \rho_{\text{obs}} \{ SC(\Delta y_1, H_o + \Delta z) - SC(\Delta y_1, H_1) + SC(\Delta y_1, H_1) - SC(L_1, H_1) + SC(L_1, \Delta z) - SC(\Delta y_1, \Delta z) + SC(\Delta y_2, H_o + \Delta z) - SC(\Delta y_2, H_1) + SC(\Delta y_2, H_1) - SC(L_2, H_1) + SC(L_2, \Delta z) - SC(\Delta y_2, \Delta z) \} \quad (15)$$

In configuration (3), cf. Figure 3c, the ERC at P reads:

$$SC_P = \rho_{\text{obs}} \{ SC(L_o + \Delta y, H_o - \Delta z) - SC(\Delta y, H_o - \Delta z) + SC(\Delta y, H) - SC(L_o + \Delta y, H) + SC(L_o + \Delta y, H) - SC(L_1, H) \} \quad (16)$$

In configuration (4), cf. Figure 3d, the ERC at P reads:

$$SC_P = \rho_{\text{obs}} \{ SC(\Delta y_1, z_{o2} - z_P) - SC(\Delta y_1, H) + SC(\Delta y_1, H) - SC(L_1, H) + SC(\Delta y_2, z_{o2} - z_P) - SC(\Delta y_2, H) + SC(\Delta y_2, H) - SC(L_2, H) \} \quad (17)$$

### 2.3. Daylight Factor

Suppose now there are also reflections from the interior surfaces (i.e., the room is not entirely black) that contribute to the horizontal illuminance value at the calculation point P. The so-called internally reflected component (IRC) is thus defined as the ratio between the illuminance contribution from the internal reflections and  $E_{\text{out}}$ . The IRC is typically assumed as a single value throughout the indoor space, i.e., it does not depend on the coordinate of the calculation point. The value depends on various parameters, namely the glazing transmittance  $\tau_g$ ; the actual daylight opening area  $A_o$ ; the total room surface area (including the opening)  $A$ ; the area-weighted mean room surface reflectance  $R$ , the area-weighted mean floor and lower walls reflectance, below the middle height of the opening, excluding the façade ( $R_{fw}$ ); the area-weighted mean ceiling and upper walls reflectance, above the middle height of the opening, excluding the façade ( $R_{cw}$ ); and the coefficient  $C$  that depends on the external obstruction angle. The IRC equation reads:

$$IRC = \frac{\tau_g A_o}{A(1 - R)} (CR_{fw} + 5R_{cw}) \quad (18)$$

The sum of SC, ERC, and IRC at the calculation point P is known as the daylight factor (DF) at P, according to the split-flux method [34]. In an actual situation, corrections may be applied to the predicted DF values due to maintenance factors ( $M$ , between 0.5 and 0.9), glass factors ( $G$ , between 0.55 and 1), and bars or framing factors ( $B$ , between 0.65 and 0.85) [35], so that:

$$DF_{P(\text{actual})} = M \cdot G \cdot B (SC_P + ERC_P + IRC) \quad (19)$$

The DF, which is also the ratio between total indoor illuminance at P ( $E_{\text{in,P}}$ ) and  $E_{\text{out}}$ , has been adopted in many national standards and building codes around the world as a practical measure of daylighting performance in indoor spaces.

Given a certain room, it is common to evaluate the DF at several calculation or sensor points on the workplane so that the spatially averaged value ( $DF_{\text{av}}$ ) can be obtained to indicate daylight availability in the room. The DF at any point inside the room and the  $DF_{\text{av}}$  are known as 'static' metrics because the values are not expected to change with respect to façade orientation and site location, so long as the room geometry is unchanged, and the assumption of the standard CIE overcast sky prevails.

### 2.4. Climate-Based Daylight Metrics

While the standard CIE overcast sky model is typically considered only in the prediction of static daylight metrics, to some extent, the model can also be employed to predict

the climate-based daylight metrics. The concept has been proposed and validated in the literature [36] to predict the so-called minimum daylight autonomy ( $DA_{\min}$ ), which is derived from the estimation of solar altitude and azimuth throughout the year using the standard CIE overcast sky, instead of the Perez (all weather) sky model distribution.

In this study, however, it is proposed to observe the typical annual profile of outdoor diffuse daylight illuminance ( $E_{\text{out}}$ ) in the building site location. Such profiles may be available in national standards (e.g., the former BS 8206-2:2008 [29]) and are practical for climates with pre-dominantly overcast sky [37–39]. By observing the profile, one can obtain the probability of any specified  $E_{\text{out}}$  values being exceeded in a typical year under the overcast sky model. The annual exceedance probability  $P_{\text{ex}}$  can be described as a function of  $E_{\text{out}}$ , i.e.,  $P_{\text{ex}} = F(E_{\text{out}})$ . However,  $E_{\text{out}}$  and the total indoor illuminance at any calculation point P (i.e.,  $E_{\text{in,P}}$ ) are proportional by the factor of  $DF_P$ . Therefore, given a certain  $E_{\text{in}}$  target value and having known the DF value at P, the annual probability of exceeding  $E_{\text{in}}$  is equal to the annual probability of exceeding the corresponding  $E_{\text{out}}$ . One can thus write:

$$P_{\text{ex}}|_{E_{\text{out,P}}} = P_{\text{ex}}|_{(E_{\text{in,P}}/DF_P)} = F\left(\frac{E_{\text{in,P}}}{DF_P}\right) \quad (20)$$

Using this model, the following climate-based daylight metrics can be predicted for any calculation point P inside the room:

- (1) Daylight autonomy, 300 lx threshold (referring to the LEED v4.1 recommendation [40]) ( $DA_{300}$ ):

$$DA_{300} = P_{\text{ex}}|_{300 \text{ lx}} = F\left(\frac{300 \text{ lx}}{DF_P}\right) \quad (21)$$

- (2) Useful daylight illuminance, autonomous (100–2000 lx, i.e., the original range proposed by [41]) (UDI-a):

$$UDI - a = P_{\text{ex}}|_{2000 \text{ lx}} - P_{\text{ex}}|_{100 \text{ lx}} = F\left(\frac{2000 \text{ lx}}{DF_P}\right) - F\left(\frac{100 \text{ lx}}{DF_P}\right) \quad (22)$$

- (3) Useful daylight illuminance, autonomous (300–3000 lx, i.e., the new range proposed by [42]) (UDI-a’):

$$UDI - a' = P_{\text{ex}}|_{3000 \text{ lx}} - P_{\text{ex}}|_{300 \text{ lx}} = F\left(\frac{3000 \text{ lx}}{DF_P}\right) - F\left(\frac{300 \text{ lx}}{DF_P}\right) \quad (23)$$

- (4) Useful daylight illuminance, exceeded (>2000 lx, i.e., the original range) (UDI-e):

$$UDI - e = P_{\text{ex}}|_{2000 \text{ lx}} \quad (24)$$

- (5) Useful daylight illuminance, exceeded (>3000 lx, i.e., the new range) (UDI-e’):

$$UDI - e' = P_{\text{ex}}|_{3000 \text{ lx}} \quad (25)$$

Based on the obtained climate-based metrics at each calculation point on the work-plane in the observed room, one can proceed to estimate spatial metrics, such as the spatial daylight autonomy with 300 lx threshold in at least 50% of the time in a year ( $sDA_{300/50\%}$ ), so that:

$$sDA_{300/50\%} \approx \frac{n_{DA_{300} \geq 50\%}}{n_{\text{tot}}} \cdot 100\% \quad (26)$$

where  $n_{DA_{300} \geq 50\%}$  is the number of points satisfying  $DA_{300} \geq 50\%$ , and  $n_{\text{tot}}$  is the total number of calculation points. With analogy to  $sDA_{300/50\%}$ , one can also estimate the spatial version of the aforementioned UDI metrics, i.e.,  $sUDI-a_{50\%}$ ,  $sUDI-a'_{50\%}$ ,  $sUDI-e_{50\%}$ , and  $sUDI-e'_{50\%}$  [27,39], all having a temporal threshold of 50%.

### 2.5. Annual Lighting Energy Demand

Annual lighting energy demand (ED) is hereby defined as the total demand for electrical lighting energy in a year, in kWh/m<sup>2</sup>/yr. The procedure to estimate ED in this study follows the assumption of an ideal, linear dimming system [39,43], in which a certain value of lighting power density (LPD (W/m<sup>2</sup>)) is assumed for the observed room. Having known the annual  $E_{out}$  profile of the site location and having computed the DF at the entire calculation points in the room, the indoor illuminance  $E_{in}$  at each point can be computed. The  $E_{out}$  value exceeded at 50% of the time is taken in this case to represent the median scenario.

Any calculation point with  $E_{in} < 300$  lx is considered in need of supplementary electric lighting, which in turn requires electrical energy. The values of  $(300 \text{ lx} - E_{in})$  at the calculation points that require supplementary lighting are then averaged. The average value is divided by  $\eta$ , which is the ratio between the target illuminance and the LPD. The obtained value is then multiplied by the total working hours in a year ( $T$ ), and is finally divided by 1000 to convert the unit to kWh, so that:

$$ED \text{ (kWh/m}^2 \text{ /yr)} = \frac{1}{m} \sum_{i=1}^m (300 - E_{in,i}) \cdot \frac{1}{\eta} \cdot \frac{T}{1000} \quad (27)$$

where  $m$  is the number of calculation points with illuminance below 300 lx, with reference to the recommended threshold in LEED v4.1 [40]. When the  $E_{in}$  values are estimated with respect to the  $E_{out}$  value satisfying  $P_{ex} = 50\%$ , the resulting annual lighting energy demand can be properly written as  $ED_{50\%}$ .

## 3. Methods

### 3.1. Room Settings

To evaluate whether the introduction of façade thickness may create an impact on the aforementioned daylight metrics and annual lighting energy demand, an isolated room with internal measures of 6 m × 4 m × 3 m is considered. The size of the room originally refers, with slight adjustments, to the size of the reference office of van Dijk and Platzer [25], which was also later adopted in more recent studies [27,39]. Thirty-five illuminance calculation points are evenly placed on the workplane inside the room, at 0.75 m above the floor (Figure 4).

A rectangular daylight opening with actual length  $L_o$  and actual height  $H_o$  high is placed centred on the 4 m × 3 m façade, which has a thickness of  $f$ . The ratio between  $L_o$  and  $H_o$  is set constant as 4:3, following the aspect ratio of the façade. The room is assumed to sit under the standard CIE overcast sky, which is rotationally symmetrical so that the façade orientation is irrelevant for the calculation. No external obstructions and shading devices are assumed, other than the thick part of the façade itself.

The room interior surface reflectances are set to 0.8, 0.5, and 0.2, respectively, for the ceiling, walls, and floor. The thick part of the façade is assumed to have a reflectance of 0.2. For the IRC calculation, the glazing is assumed to have 0.85 visible transmittance, and the  $C$  coefficient is assumed to be 39 (i.e., no external obstruction angle [44]). The DF correction factors are set as follows:  $M = 0.90$  (vertical opening in a relatively clean room at a non-industrial area),  $G = 1.00$  (clear glass), and  $B = 0.85$ , assuming the largest suggested values in reference [35].

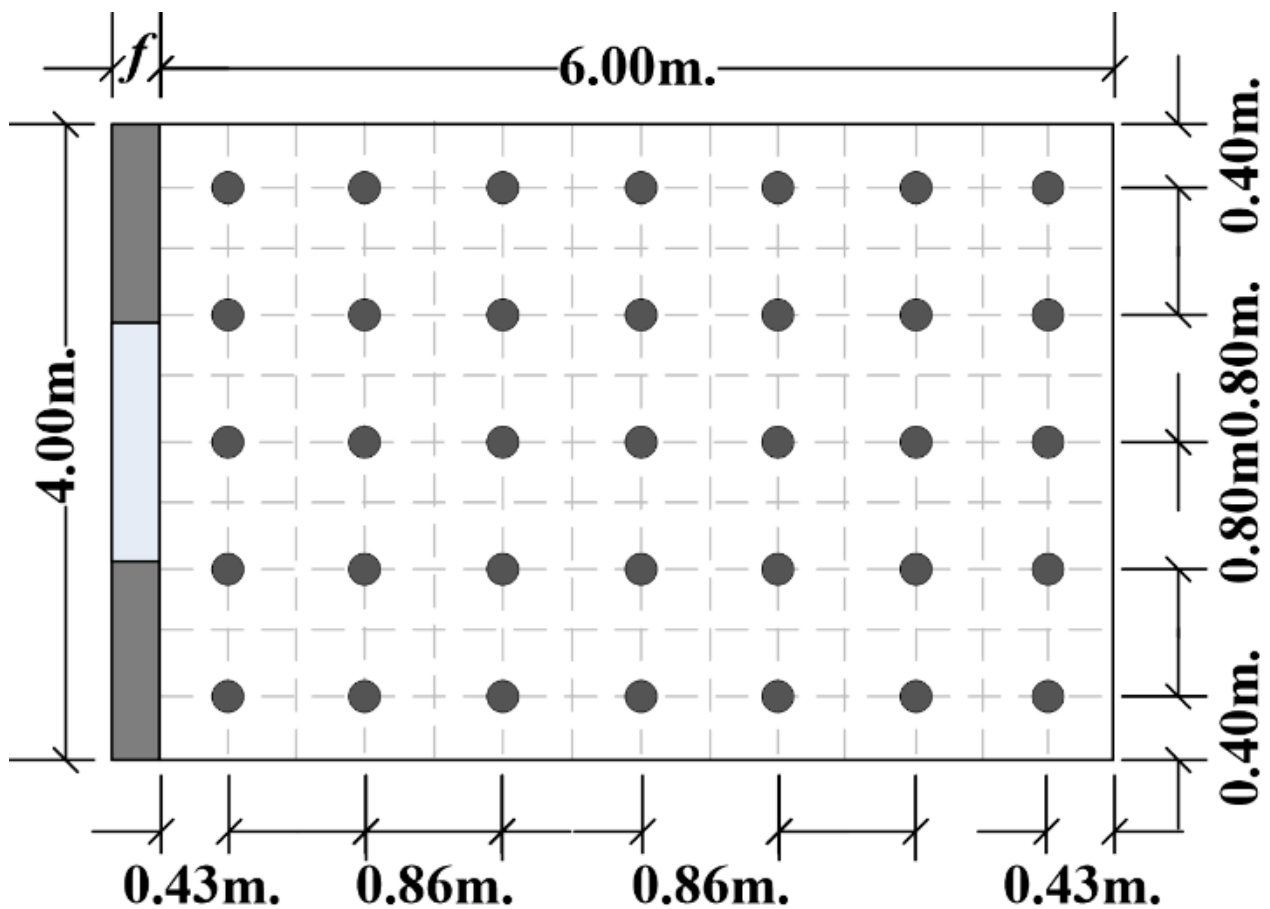


**Figure 4.** Plan view of the observed room with a façade thickness  $f$ , together with the defined 35 workplane illuminance calculation points.

### 3.2. Annual Daylight Profile

For the purpose of estimating the climate-based daylight metrics, the site location of the room is set as Makassar, Indonesia ( $5^{\circ}8' S$ ,  $119^{\circ}25' E$ ). The city is located in the Am (tropical monsoon) region according to the Köppen–Geiger climate classification, with an elevation of around 0–25 m above sea level. This city is particularly chosen since long-term measurement data of solar irradiance and daylight illuminance for the city are available since the 1990s; through the International Daylight Measurement Programme (IDMP) [37,38]. Geographically speaking, Makassar is located in a coastal area, as is the case for the majority of large cities in Indonesia, and thus shall be sufficiently representative.

The typical annual profile of  $E_{out}$  can be drawn (Figure 5) based on the provided data with the  $P_{ex}$  interval of 1% [37], for the time frame between 09.00 and 17.00 h each day. The 100% exceedance probability corresponds to  $E_{out} = 6000$  lx or lower;  $P_{ex} = 50\%$  corresponds to  $E_{out} = 30,070$  lx; and  $P_{ex} = 0\%$  corresponds to  $E_{out} = 79,000$  lx or higher. Hereinafter, the first value is called the lowermost  $E_{out}$  (i.e.,  $E_{out,low}$ ), the middle value is the median  $E_{out}$  (i.e.,  $E_{out,med}$ ), and the last value is the uppermost  $E_{out}$  (i.e.,  $E_{out,up}$ ).

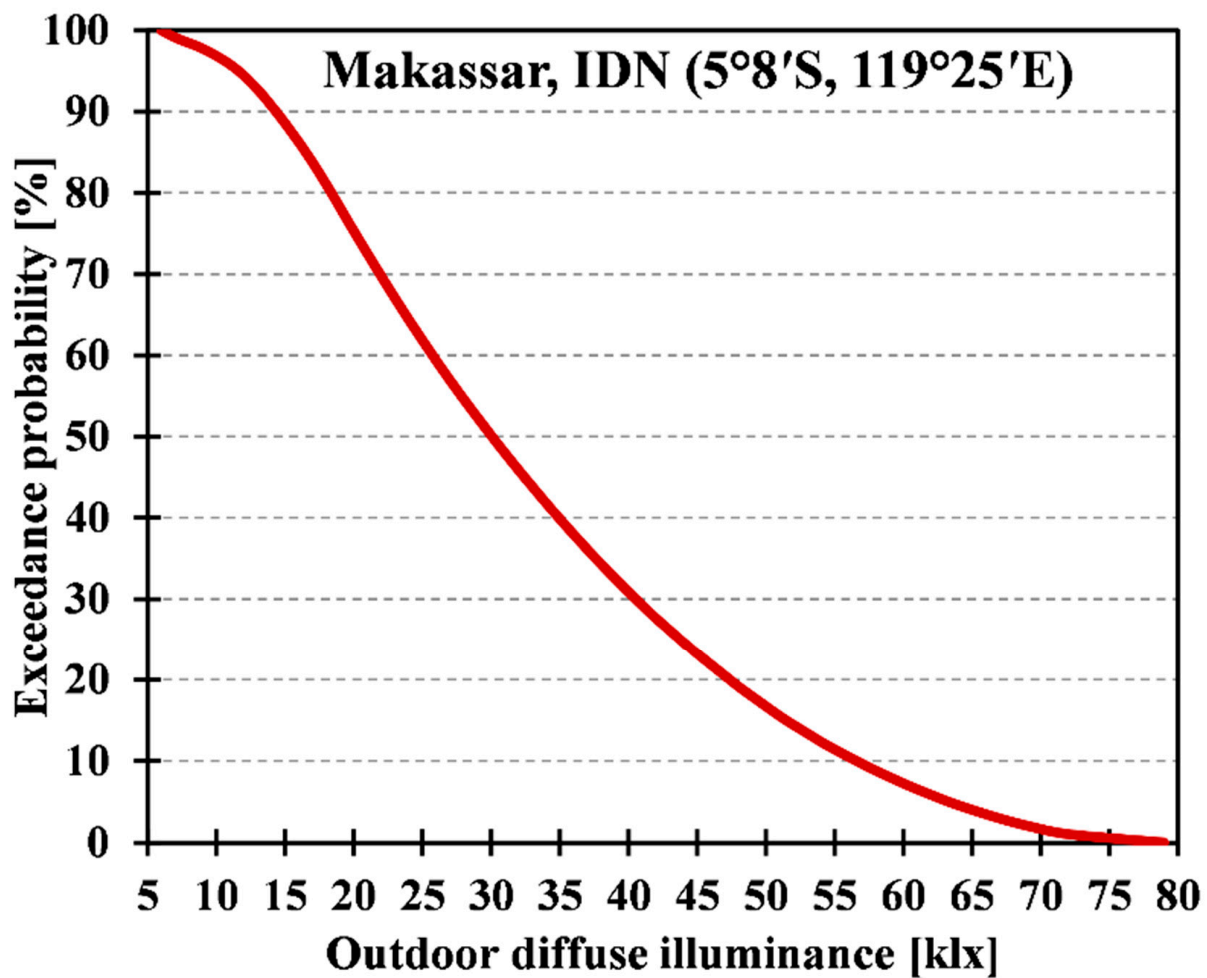


**Figure 5.** Annual exceedance probability of outdoor daylight diffuse illuminance at 09.00–17.00 h in the city of Makassar, Indonesia; adapted from [39].

To estimate the climate-based metrics as described in Section 2.4, it is important to determine the  $P_{ex}$  values that correspond to the threshold illuminance ( $E_t$ ) of 100, 300, 2000, and 3000 lx at each calculation point. However, given a certain opening configuration, one shall start with computing the DF values. Having known the DF value at a certain point, one would wish to directly estimate the annual probability of exceeding a certain  $E_t$  value so that the climate-based metrics can be computed for that point. In other words, it shall be practical to represent the  $P_{ex}$  as a function of DF at various threshold illuminances. To do so, it is first required to have the relation between the  $P_{ex}$  and the normalised outdoor illuminance ( $\xi$ ) values. The latter is defined as the ratio between a given  $E_{out}$  value and the  $E_{out,up}$  in the annual profile. In the case of  $E_{out} > E_{out,up}$ , the  $\xi$  is defined as 1.

$$\xi = \begin{cases} \frac{E_{out}}{E_{out,up}}, & E_{out} \leq E_{out,up} \\ 1, & E_{out} > E_{out,up} \end{cases} \quad (28)$$

The  $E_{out}$  values in Figure 5 are thus converted to  $\xi$ , with respect to the  $E_{out,up} = 79,000$  lx. Since  $E_{out,low} = 6000$  lx, the smallest  $\xi$  is thus  $\approx 0.0759$ . After performing the appropriate polynomial regression, the relation between  $P_{ex}$  and  $\xi$  for the given annual profile ( $\xi \in [0.0759, 1]$ ) reads:

$$P_{ex} = -2376.1353 \xi^6 + 8738.9044 \xi^5 - 12,877.7845 \xi^4 + 9642.6051 \xi^3 - 3674.2889 \xi^2 + 465.5675 \xi + 81.0071; R^2 = 0.9999 \quad (29)$$

Provided a certain threshold illuminance  $E_t$  and having known the DF at the calculation P, the corresponding  $\xi$  can be determined as follows:

$$\xi = \begin{cases} 0.0759, & E_t/DF_P < E_{out,low} \\ \frac{E_t}{DF_P \cdot E_{out,up}}, & E_{out,low} \leq E_t/DF_P \leq E_{out,up} \\ 1, & E_t/DF_P > E_{out,up} \end{cases} \quad (30)$$

The obtained  $\xi$  value is thus inserted to Equation (29) to yield  $P_{ex}$  for the calculation P, with respect to the defined  $E_t$ . To create graphical representations of the relationship, several variations of DF are introduced, ranging from 0.1% to 50%, with  $E_t = 100, 300, 2000,$  and  $3000$  lx. The resulting graphs between  $P_{ex}$  and DF for the four  $E_t$  values are displayed in Figure 6. Whenever necessary, linear interpolation may be applied between two adjacent points on the graphs to estimate the  $P_{ex}$ . Having known the relation between  $P_{ex}$  and DF, one can thus proceed with the estimation of climate-based metrics as desired.

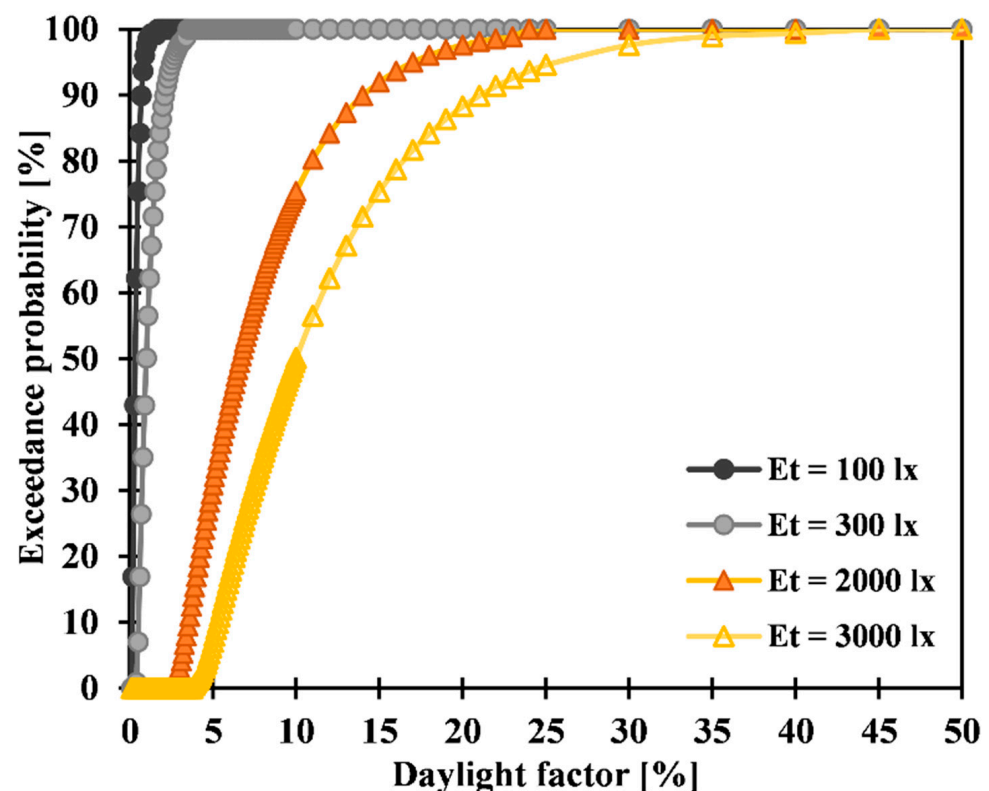


**Figure 6.** Annual exceedance probability of threshold illuminance of 100, 300, 2000, and 3000 lx, provided various DF values in a room, based on the annual daylighting profile of Makassar, Indonesia.

### 3.3. Sensitivity and Uncertainty Analyses

Various façade thickness  $f$  from 0 to 0.50 m, with an interval of 0.05 m, are considered in this study. Theoretical calculations are performed for three different WWR, namely 25%, 50%, and 75%, to represent typically small, medium, and large opening areas.

Several output variables or metrics are reported and observed in this study, i.e.:

- (1) Metrics at the central calculation point (cf. Figure 4), which include: DF,  $DA_{300}$ , UDI-a, UDI-a', UDI-e, and UDI-e'.
- (2) Metrics for the entire room, based on all calculation points in Figure 4, which include:  $DF_{av}$ ,  $sDA_{300/50\%}$ ,  $sUDI-a_{50\%}$ ,  $sUDI-a'_{50\%}$ ,  $sUDI-e_{50\%}$ ,  $sUDI-e'_{50\%}$ , and  $ED_{50\%}$ .

To observe the sensitivity of each metric with respect to varying  $f$ , scatter plots of the metrics are drawn at each WWR. Plots with steeper gradients shall indicate higher

sensitivity to the variation of façade thickness. Furthermore, each metric value at  $f = 0$  is compared to the value at  $f = 0.25$  and  $0.50$  m, where ratios closer to unity indicate a lower impact of façade thickness. One can thus compute the estimation error  $\varepsilon$  when  $f$  is neglected, which in this case is defined as follows:

$$\varepsilon = \left| \frac{\text{Estimated metric value at } f = 0}{\text{Actual metric value at } f > 0} - 1 \right| \quad (31)$$

To quantify the effect of uncertainty, the coefficient of variation (CV), i.e., the ratio between standard deviation and mean values, is also evaluated across  $f$  at each WWR. Smaller CV values indicate less uncertainty of the outcome when  $f$  is not exactly known.

Moreover, the minimum, three quartiles ( $Q_1$ ,  $Q_2$ ,  $Q_3$ ), and maximum values of each metric are reported as boxplots to observe the uncertainty due to all possible variations of  $f$ . In addition, the interquartile range (IQR) is also computed. The smaller the IQR, the smaller the resulting uncertainty of the metric.

## 4. Results

### 4.1. Sensitivity Analysis

To observe the sensitivity with respect to façade thickness  $f$ , Figure 7 displays the relationship between the obtained metrics at the central calculation point in the modelled room as a function of  $f$ . It is observed that variation of  $f$  yields different impacts on the daylight metrics, but the degree of the impact also depends on the relative size of the opening area (WWR). For example, with regard to DF (Figure 7a), the greater the façade thickness, the smaller the DF, but the trend is more visible at WWR 75%, i.e., in scenes with a large opening area. With regard to  $DA_{300}$  (Figure 7b), the impact of  $f$  is more visible at WWR 25%, i.e., in scenes with a small opening area. In scenes with a large opening area, the threshold illuminance of 300 lx has been achieved so that the metric is saturated, regardless of the façade thickness.

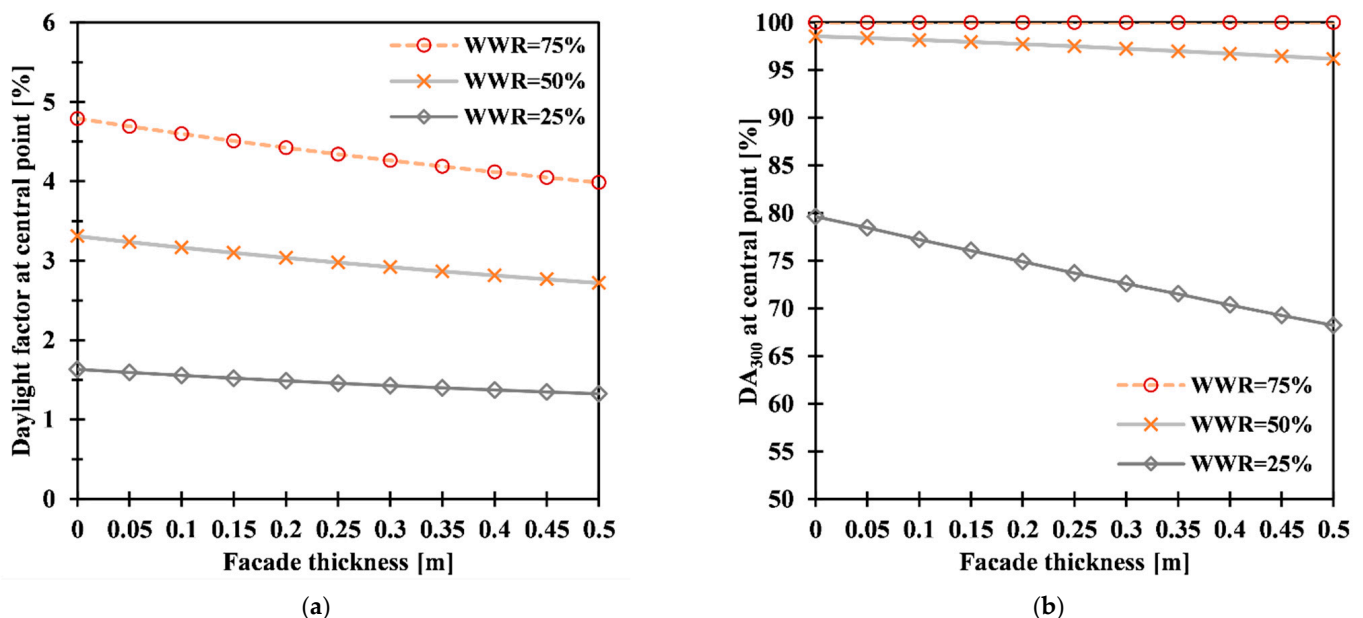
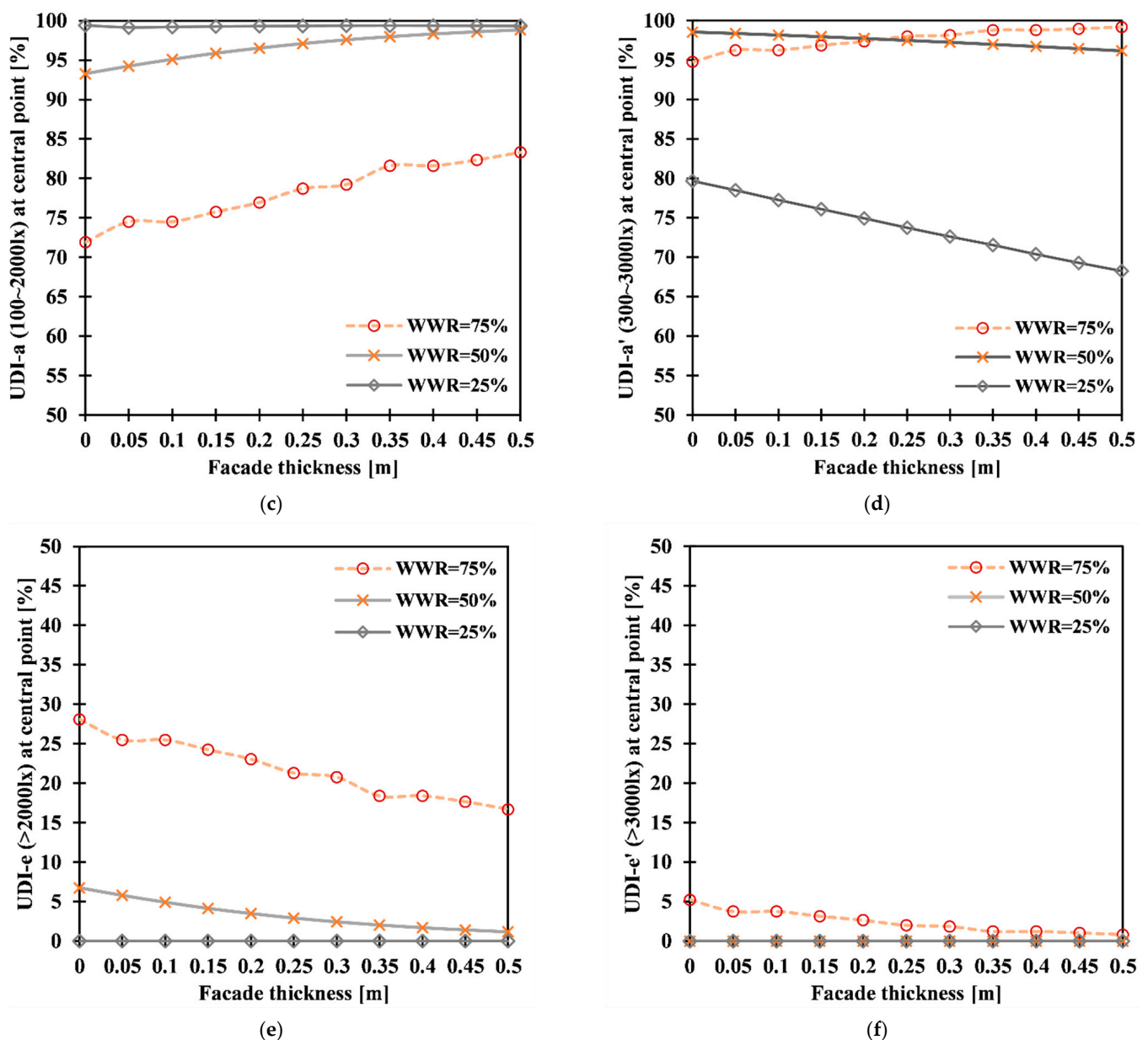


Figure 7. Cont.



**Figure 7.** Resulting daylight metrics: (a) DF, (b)  $DA_{300}$ , (c) UDI-a, (d) UDI-a', (e) UDI-e, and (f) UDI-e' at the central point due to various façade thicknesses.

With regard to UDI-a (Figure 7c), in scenes with a small opening area, the values are maintained at 100%, regardless of the façade thickness. In other words, the workplane illuminance at the central point is always well within the range of 100–2000 lx. In scenes with a large opening area, the upper threshold of 2000 lx is exceeded so that the resulting UDI-a becomes smaller. In that case, increasing the façade thickness shall reduce the effective daylight opening so that the UDI-a becomes larger, hence the positive gradient.

Interestingly, altering the useful illuminance range will also change the sensitivity trend. The graph of UDI-a' (Figure 7d), which apply 300–3000 lx as the target range, suggests that the trend gradient is negative at WWR 25%, is almost flat at WWR 50%, and is positive at WWR 75%.

Table 1 displays the ratios between each metric value at  $f = 0$  and at  $f = 0.25$  or  $0.50$  m at each WWR. The bold-printed numbers represent unity, i.e., the compared values are exactly the same. It is found that UDI-a is the least affected by the variation of  $f$ . At WWR 25%, assuming  $f = 0$ , yields the UDI-a value that is just the same as the value at  $f = 0.25$  m.

In other words, neglecting the façade thickness, in that case, shall result in practically zero error. At WWR 75%, assuming  $f = 0$  yields 9% lower UDI-a than when  $f = 0.25$  m is assumed, or about 9% error if the thickness is ignored.

**Table 1.** Ratio between each metric value at the central point at  $f = 0$  and  $f = 0.25$  m or  $0.50$  m.

WWR (%)	Ratio between Value at $f = 0$ and $f = 0.25$ m					
	DF	DA300	UDI-a	UDI-a'	UDI-e	UDI-e'
25	1.12	1.08	1.00	1.08	n/a	n/a
50	1.11	1.01	0.96	1.01	2.32	n/a
75	1.10	1.00	0.91	0.97	1.32	2.62
WWR (%)	Ratio between Value at $f = 0$ and $f = 0.50$ m					
	DF	DA300	UDI-a	UDI-a'	UDI-e	UDI-e'
25	1.23	1.17	1.00	1.17	n/a	n/a
50	1.22	1.02	0.94	1.02	5.84	n/a
75	1.20	1.00	0.86	0.96	1.68	6.44

n/a: both compared values or the denominator are zero.

With regard to  $DA_{300}$ , in scenes with a medium or large opening area, neglecting the façade thickness shall yield less than 2% error, which is insignificant. A relatively large error (around 17% overestimation) for  $DA_{300}$  only occurs in scenes with a small opening area.

Meanwhile, with regard to DF, the errors when  $f$  is neglected are consistent at around 10–12%, where slightly smaller errors are expected in the presence of a large opening area. In terms of UDI-e and UDI-e', as also observed in Table 1, the comparison is irrelevant in cases with a small opening area. In cases with a large opening area, the estimation errors of UDI-e and UDI-e' are expected to be great, i.e., more than 100%. This is due to the small quantity of the metrics (cf. Figure 7e,f), which makes the number seems highly sensitive to small changes.

Figure 8 displays the relationship between the obtained metrics for the entire room to various façade thicknesses. As in the results of the metrics for the central point, the variation of façade thickness also yields a different impact on the daylight metrics. Most of the plots in Figure 8 have more fluctuations than those in Figure 7, because Figure 8 represents the spatial metrics for the entire room, which involve all calculation points that may average each other, so that the trend is less monotonous compared to the metrics for a single point.

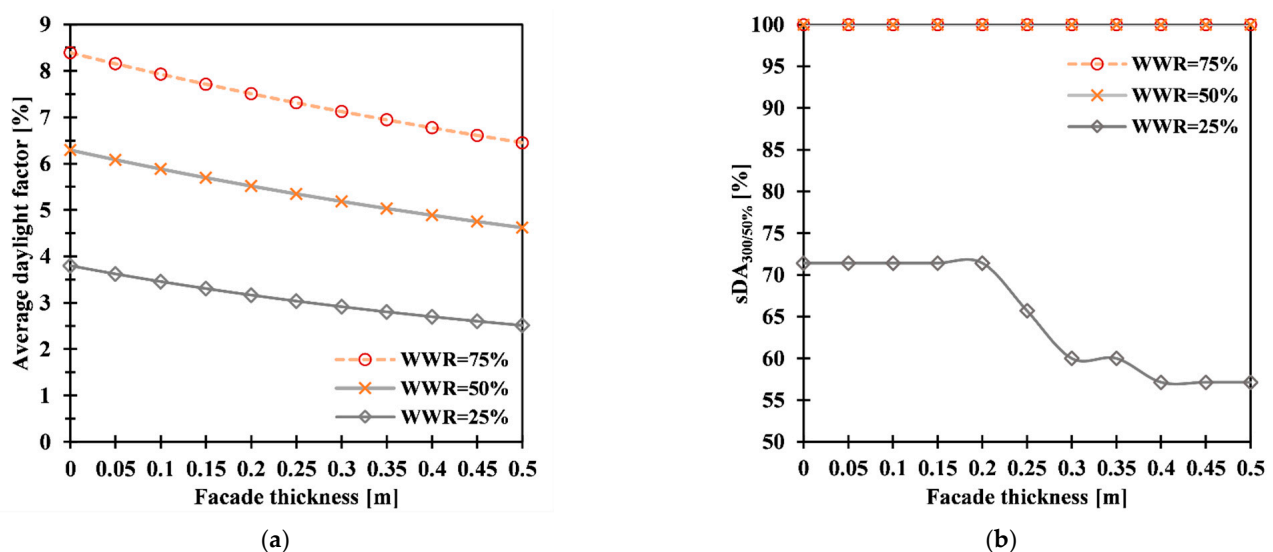
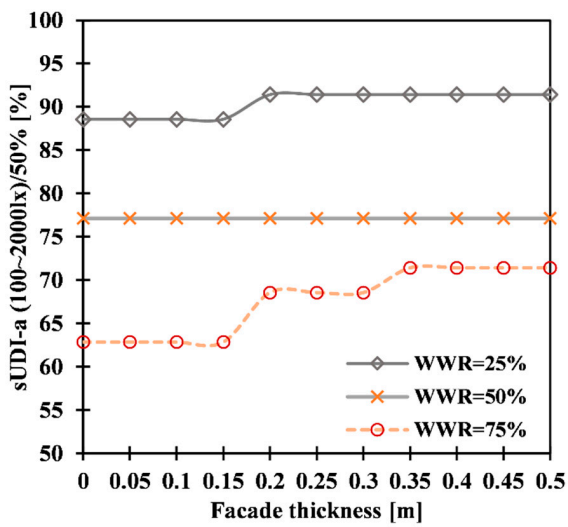
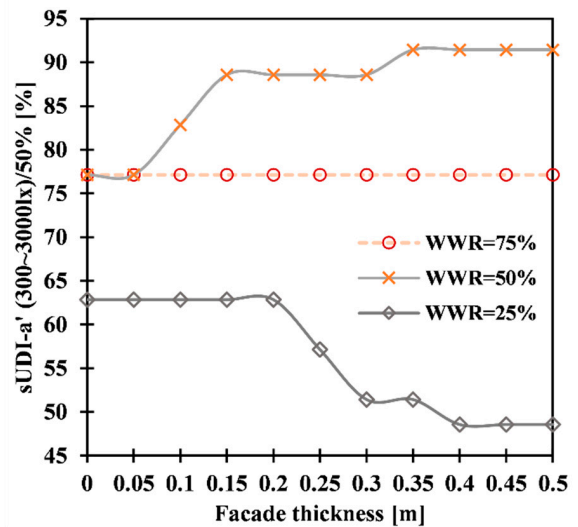


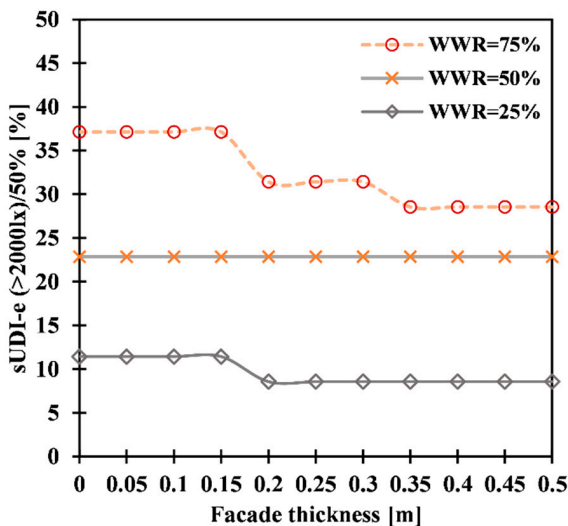
**Figure 8.** Cont.



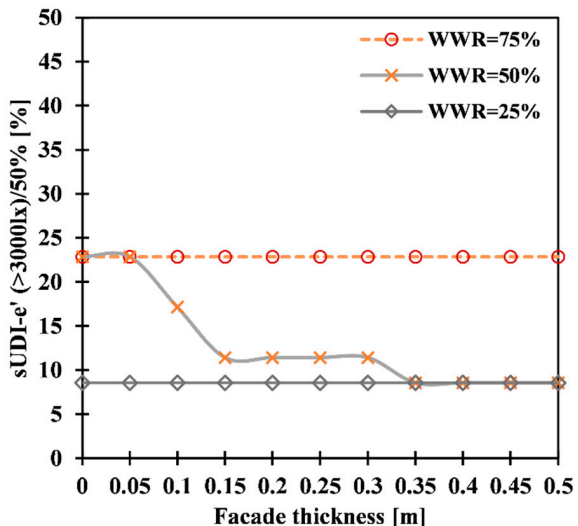
(c)



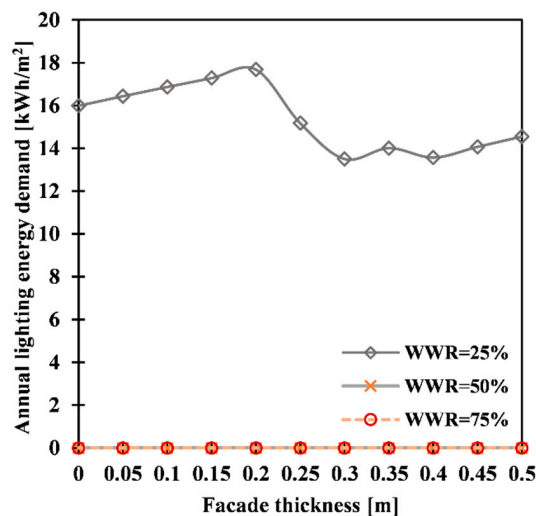
(d)



(e)



(f)



(g)

Figure 8. Resulting daylight metrics: (a)  $DF_{av}$ , (b)  $sDA_{300/50\%}$ , (c)  $sUDI-a_{50\%}$ , (d)  $sUDI-a'_{50\%}$ , (e)  $sUDI-e_{50\%}$ , (f)  $sUDI-e'_{50\%}$ , and (g)  $ED_{50\%}$  in the entire room due to various façade thicknesses.

The sensitivity trends may also vary in different scenes with different opening area sizes. For example, the  $sUDI-a_{50\%}$  (Figure 8c) and  $sUDI-a'_{50\%}$  (Figure 8d) values initially increase when the WWR is getting larger; but decrease again when the WWR is larger than the optimum values. The  $ED_{50\%}$  values are zero in scenes with a medium or large opening area, regardless of the façade thickness, because the workplane illuminance at all calculation points in that case already exceeds 300 lx; thus, no supplementary electric lighting is required.

Table 2 suggests a similar tendency with Table 1, with  $sDA_{300/50\%}$  being the least affected by the variation of  $f$ , having the ratios of exactly 1 in scenes with a medium or large opening area. Moreover, the ratios for  $sUDI-a_{50\%}$  in Table 2 are relatively small, within 0.92–1.00 in comparison to  $f = 0.25$  m, and within 0.88–1.00 in comparison to  $f = 0.50$  m.

**Table 2.** Ratio between each metric value for the entire room at  $f = 0$  and  $f = 0.25$  m or  $0.50$  m.

WWR (%)	Ratio between Value at $f = 0$ and $f = 0.25$ m						
	$DF_{av}$	$sDA_{300/50\%}$	$sUDI-a_{50\%}$	$sUDI-a'_{50\%}$	$sUDI-e_{50\%}$	$sUDI-e'_{50\%}$	$ED_{50\%}$
25	1.25	1.09	0.97	1.10	1.33	1.00	1.05
50	1.18	1.00	1.00	0.87	1.00	2.00	n/a
75	1.15	1.00	0.92	1.00	1.18	1.00	n/a
WWR (%)	Ratio between Value at $f = 0$ and $f = 0.50$ m						
	$DF_{av}$	$sDA_{300/50\%}$	$sUDI-a_{50\%}$	$sUDI-a'_{50\%}$	$sUDI-e_{50\%}$	$sUDI-e'_{50\%}$	$ED_{50\%}$
25	1.51	1.25	0.97	1.29	1.33	1.00	1.10
50	1.36	1.00	1.00	0.84	1.00	2.67	n/a
75	1.30	1.00	0.88	1.00	1.30	1.00	n/a

n/a: both compared values or the denominator are zero.

Meanwhile, the ratios for  $DF_{av}$  are within 1.15–1.25 in comparison with  $f = 0.25$  m, and within 1.30–1.51 in comparison with  $f = 0.50$  m. The ratios tend to become smaller in scenes with a large opening area. The remaining metrics have fluctuating ratios since all calculation points are considered in the computation. On the contrary, when evaluated at only a single point, the metric values tend to consistently increase or decrease as the WWR increases.

#### 4.2. Uncertainty Analysis

The CV values of each metric at the central calculation point across all façade thicknesses  $f$  are summarised in Table 3, in which the bold-printed numbers indicate  $CV = 0$ , i.e., no deviation at all from the mean value. Table 3 suggests that several metrics, namely  $DA_{300}$ ,  $UDI-a$ , and  $UDI-a'$ , yield relatively small CVs and thus are the least affected by the change of  $f$ . In particular,  $DA_{300}$  and  $UDI-a$  have the most consistently small CV, ranging from 0 to 0.05.

**Table 3.** Coefficient of variation of each metric at the central point across façade thickness.

WWR (%)	Coefficient of Variation (-)					
	DF	$DA_{300}$	UDI-a	UDI-a'	UDI-e	UDI-e'
25	0.07	0.05	0.00	0.05	n/a	n/a
50	0.07	0.01	0.02	0.01	0.56	n/a
75	0.06	0.00	0.05	0.01	0.17	0.58

n/a: both the standard deviation and the mean values are zero.

Meanwhile, the greatest CV values (0.58) are found for  $UDI-e'$ , particularly in scenes with a large opening area. In scenes with a small opening area,  $UDI-e$  and  $UDI-e'$  are irrelevant because the upper threshold illuminance is never exceeded in those scenes, as also depicted in Figure 7e,f.

Table 4 summarises the CV values of the obtained metrics for the entire room across  $f$  at various WWRs. It is observed that  $sDA_{300/50\%}$  has the most occurrences of zero CV, which are achieved in scenes with a medium or large opening area, meaning that the  $sDA_{300/50\%}$  values shall remain unchanged despite the uncertainty of  $f$  in those scenarios. Next to  $sDA_{300/50\%}$ , the  $sUDI-a_{50\%}$  also has consistently small CV values, between 0 and 0.06. Both metrics are thus the ones with the lowest uncertainty.

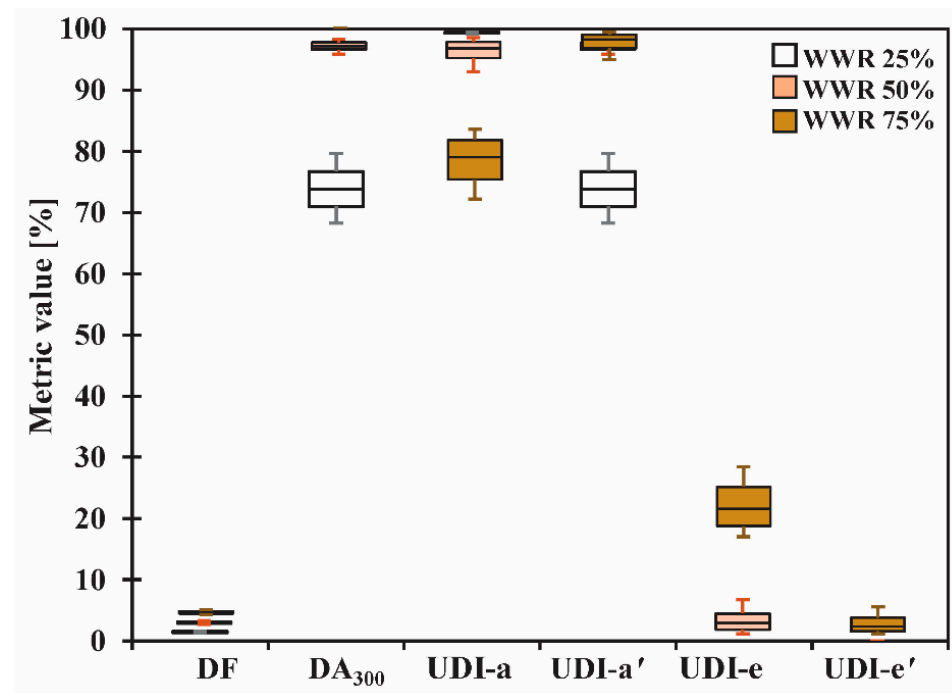
**Table 4.** Coefficient of variation of each metric for the entire room across façade thicknesses.

WWR (%)	Coefficient of Variation (-)						
	$DF_{av}$	$sDA_{300/50\%}$	$sUDI-a_{50\%}$	$sUDI-a'_{50\%}$	$sUDI-e_{50\%}$	$sUDI-e'_{50\%}$	$ED_{50\%}$
25	0.14	0.10	0.02	0.12	0.15	0.00	0.10
50	0.10	0.00	0.00	0.06	0.00	0.42	n/a
75	0.09	0.00	0.06	0.00	0.12	0.00	n/a

n/a: both the standard deviation and the mean values are zero.

With regard to  $DF_{av}$ , the CV values tend to become smaller as the WWR becomes larger. However, even at WWR 75%, the CV is still 0.09, meaning that the uncertainty of  $DF_{av}$  is higher than the uncertainties of  $sDA_{300/50\%}$  and  $sUDI-a_{50\%}$  in the same case. Meanwhile, the CV values of the annual lighting energy demand  $ED_{50\%}$  are undefined in scenes with a medium or large opening area because the workplane illuminance exceeds 300 lx at all calculation points (assuming 50% exceedance probability of the  $E_{out}$ ), yielding zero demand for supplementary electrical lighting. In scenes with a small opening area,  $ED_{50\%}$  has CV = 0.10, which is roughly the same as the CV of  $sDA_{300/50\%}$  in the same case.

To further visualise the effect of uncertainty, Figure 9 displays the boxplots depicting the minimum, the three quartiles ( $Q_1$ ,  $Q_2$ ,  $Q_3$ ), and the maximum values of each metric at the central calculation point and for the entire room due to possibly varying façade thicknesses  $f$  at each WWR value. In addition, Table 5 summarises the interquartile range of each metric.



(a)

**Figure 9.** Cont.

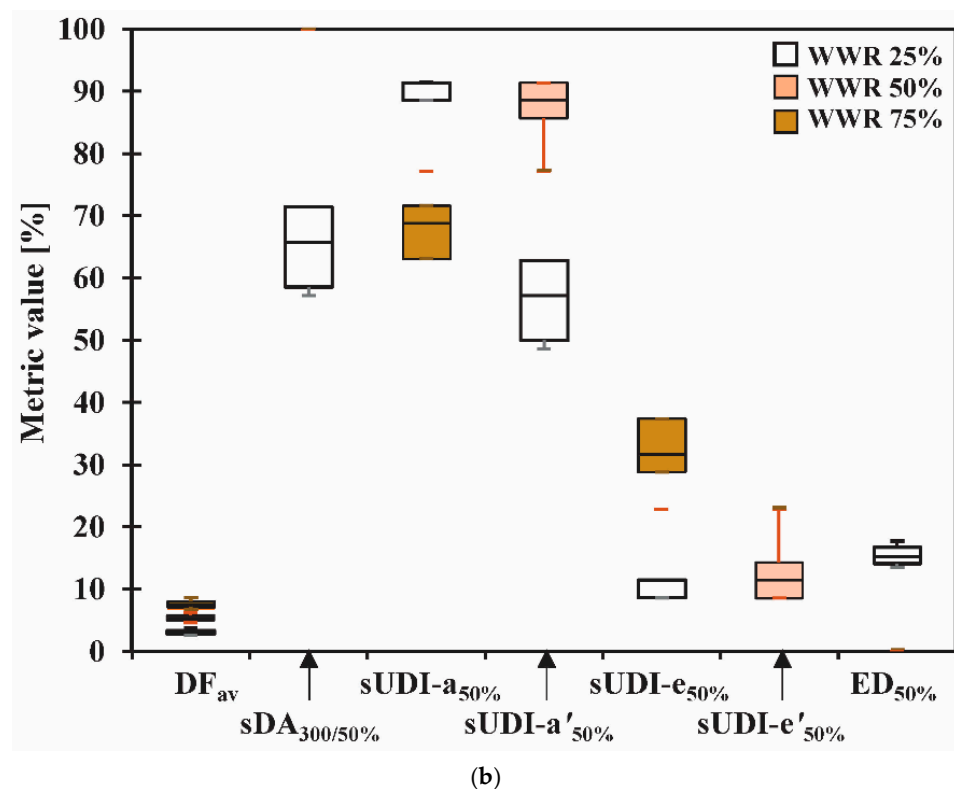


**Figure 9.** Boxplots showing the minimum,  $Q_1$ ,  $Q_2$ ,  $Q_3$ , and maximum values of each metric (a) at the central point and (b) for the entire room due to uncertain façade thickness.

**Table 5.** Interquartile range (IQR) of each metric at the central point and for the entire room due to uncertain façade thickness.

WWR (%)	IQR of Metric at the Central Point (%)							
	DF	DA <sub>300</sub>	UDI-a	UDI-a'	UDI-e	UDI-e'		
25	0.15	5.71	0.07	5.71	0.00	0.00		
50	0.29	1.20	2.67	1.20	2.67	0.00		
75	0.40	0.00	6.47	2.24	6.47	2.24		
WWR (%)	IQR of Metric for the Entire Room (%)							
	DF <sub>av</sub>	sDA <sub>300/50%</sub>	sUDI-a <sub>50%</sub>	sUDI-a' <sub>50%</sub>	sUDI-e <sub>50%</sub>	sUDI-e' <sub>50%</sub>	ED <sub>50%</sub>	
25	0.63	12.86	2.86	12.86	2.86	0.00	2.61	
50	0.83	0.00	0.00	5.71	0.00	5.71	0.00	
75	0.96	0.00	8.57	0.00	8.57	0.00	0.00	

Figure 9 and Table 4 suggest that the resulting uncertainties due to varying façade thickness are different for each metric and each WWR value. Despite all variations, among all metrics, the DF at the central point is apparently the one with the smallest uncertainty, i.e., having an IQR of no more than 0.4%. The DF<sub>av</sub> comes next, having an IQR of no more than 1%.

Some of the remaining metrics are found to have a zero IQR, meaning that the values are not changed at all in scenes with a small opening area; but the IQR becomes rather large in scenes with a large opening area. Examples of these metrics are UDI-e and UDI-e' because they are sensitive to the upper illuminance threshold (2000 or 3000 lx), which is more likely to be achieved when the WWR is large. Conversely, several other metrics have a zero IQR in scenes with a large opening area but have a large IQR in scenes with a small opening area. The DA<sub>300</sub>, sDA<sub>300/50%</sub> and ED<sub>50%</sub> are examples of this type of metric, because they are sensitive to the lower illuminance threshold (300 lx), which is critical when the WWR is small.

## 5. Discussion

### 5.1. Inter-Model Comparison

To further verify the proposed concept, an inter-model comparison is conducted referring to an earlier study that performed a simulation of the same reference office space [27]. In that study, the Perez sky model was assumed based on the weather data (EPW file) of Bandung, Indonesia, and the results were entirely obtained from annual simulation using *Daysim*. Since the EPW file was employed, the presence of direct sunlight or direct normal irradiance was also included in that study.

The WWR of the façade in that study [27] was set constant at 25% (i.e., 3 m × 1 m), and simulations were performed for each of the four façade orientations. The simulation results of  $DF_{av}$ ,  $sDA_{300/50\%}$ ,  $sUDI-a_{50\%}$ , and  $sUDI-e_{50\%}$  are shown in Table 6. The majority of the CV values across the four orientations are within no more than 0.05, suggesting small differences in the outcome due to different façade orientations. This does not necessarily imply that the real sky (or overcast sky) in the tropics is always rotationally symmetrical in a perfect way as in the standard CIE overcast sky. Differences do occur, but the figures, in this case, are negligible to some extent.

**Table 6.** Simulation results of each metric at four façade orientations based on the data from reference [27].

Metric	$f$ (m)									
	0.05	0.10	0.15	0.20	0.25	0.30	0.35	0.40	0.45	0.50
<b><math>DF_{av}</math></b>										
North	4.97	4.74	4.42	4.16	3.92	3.67	3.46	3.25	3.07	2.89
South	5.02	4.71	4.41	4.16	3.90	3.65	3.45	3.25	3.08	2.94
East	4.98	4.69	4.46	4.16	3.95	3.67	3.43	3.22	3.08	2.86
South	5.01	4.69	4.43	4.16	3.89	3.65	3.43	3.24	3.03	2.89
Average	5.00	4.70	4.43	4.16	3.91	3.66	3.44	3.24	3.07	2.89
CV	0.01	0.01	0.00	0.00	0.01	0.00	0.00	0.00	0.01	0.01
<b><math>sDA_{300/50\%}</math></b>										
North	71.4	71.4	65.7	68.6	65.7	60.0	62.9	57.1	57.1	57.1
South	71.4	71.4	68.6	65.7	65.7	62.9	57.1	57.1	57.1	57.1
East	71.4	71.4	68.6	65.7	65.7	60.0	57.1	57.1	57.1	57.1
South	71.4	71.4	71.4	71.4	68.6	65.7	62.9	62.9	57.1	57.1
Average	71.4	71.4	68.6	67.9	66.4	62.1	60.0	58.6	57.1	57.1
CV	0.00	0.00	0.03	0.04	0.02	0.04	0.05	0.05	0.00	0.00
<b><math>sUDI-a_{50\%}</math></b>										
North	82.9	91.4	91.4	91.4	91.4	91.4	91.4	91.4	91.4	94.3
South	88.6	91.4	91.4	91.4	91.4	91.4	91.4	91.4	91.4	94.3
East	85.7	88.6	88.6	91.4	91.4	91.4	91.4	91.4	91.4	91.4
South	88.6	91.4	91.4	91.4	91.4	91.4	91.4	91.4	91.4	97.1
Average	86.4	90.7	90.7	91.4	91.4	91.4	91.4	91.4	91.4	94.3
CV	0.03	0.02	0.02	0.00	0.00	0.00	0.00	0.00	0.00	0.02
<b><math>sUDI-e_{50\%}</math></b>										
North	17.1	14.3	11.4	8.6	8.6	8.6	8.6	8.6	8.6	8.6
South	11.4	8.6	8.6	8.6	8.6	8.6	8.6	8.6	8.6	5.7
East	17.1	14.3	11.4	8.6	8.6	8.6	8.6	8.6	8.6	8.6
South	11.4	8.6	8.6	8.6	8.6	8.6	8.6	8.6	8.6	2.9
Average	14.3	11.4	10.0	8.6	8.6	8.6	8.6	8.6	8.6	6.4
CV	0.23	0.29	0.16	0.00	0.00	0.00	0.00	0.00	0.00	0.43

A possible explanation for this phenomenon is the fact that in the tropics, the sun elevation angle around noon on any day of the year is typically high, i.e., near the zenith, so that the contribution of direct sunlight on the building façade around that time is relatively small. Direct sunlight on the façade is thus limited only at early or late in the day, in which the direct normal irradiance is practically smaller than that at noon. Moreover, for tropical regions located in the archipelago, the chance of having cloudy days is relatively high due

to the proximity to the ocean, which renders the assumption of the standard CIE overcast sky more realistic.

Results from the reference study in Table 6 also suggest that  $DF_{av}$  and  $sDA_{300/50\%}$  generally decrease with respect to  $f$ , while  $sUDI-a_{50\%}$  and  $sUDI-e_{50\%}$  are generally stable, agreeing with the general trend of the current study. Having known that the differences within orientations are relatively small, Figure 10 displays the results of the inter-model comparison of the average values of  $DF_{av}$ ,  $sDA_{300/50\%}$ ,  $sUDI-a_{50\%}$ , and  $sUDI-e_{50\%}$  in reference [27] and the obtained theoretical values in this study. Note that the  $M \times G \times B$  correction is not applied in the compared  $DF_{av}$  values.

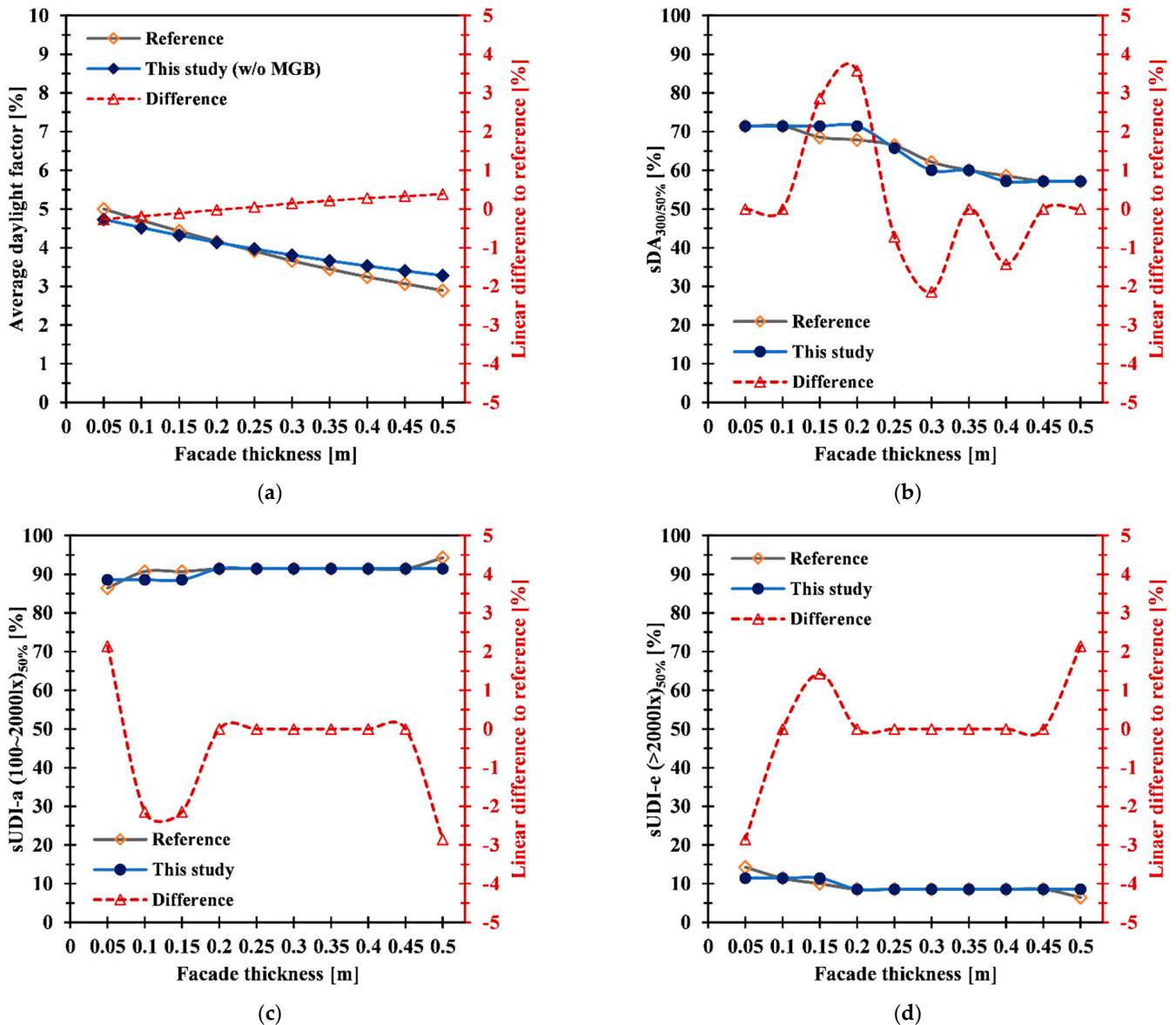


**Figure 10.** Results of inter-model comparison between the data from reference [27] and this study, for (a)  $DF_{av}$ , (b)  $sDA_{300/50\%}$ , (c)  $sUDI-a_{50\%}$ , and (d)  $sUDI-e_{50\%}$ .

The linear differences between theoretical values of  $DF_{av}$  in Makassar and simulated  $DF_{av}$  in Bandung are between  $-0.3\%$  at  $f = 0.05$  m and  $+0.4\%$  at  $f = 0.50$  m. In that case, the resulting differences are also linear across  $f$  values. Meanwhile, the linear differences between theoretical values of climate-based metrics in Makassar and simulated climate-based metrics in Bandung are within  $\pm 4\%$  (cf. Figure 10), suggesting a good agreement.

Therefore, the choice of using the outdoor daylight profile of Makassar in this study is deemed justified since it can reasonably represent the situation in other cities in an Indonesian context. It is, however, possible that locations outside the tropical climate region may not be well represented due to the difference in the climate characteristics.

### 5.2. Spatial Distribution

To visualise the spatial distributions on the workplane in the room, Figure 11 displays the spatial distribution plan of the DF calculated in this study, for each WWR and for  $f = 0$ , 0.25, and 0.50 m. Notice that the relative spatial distributions are always symmetrical, as expected due to the symmetry of the window and of the standard CIE overcast sky.

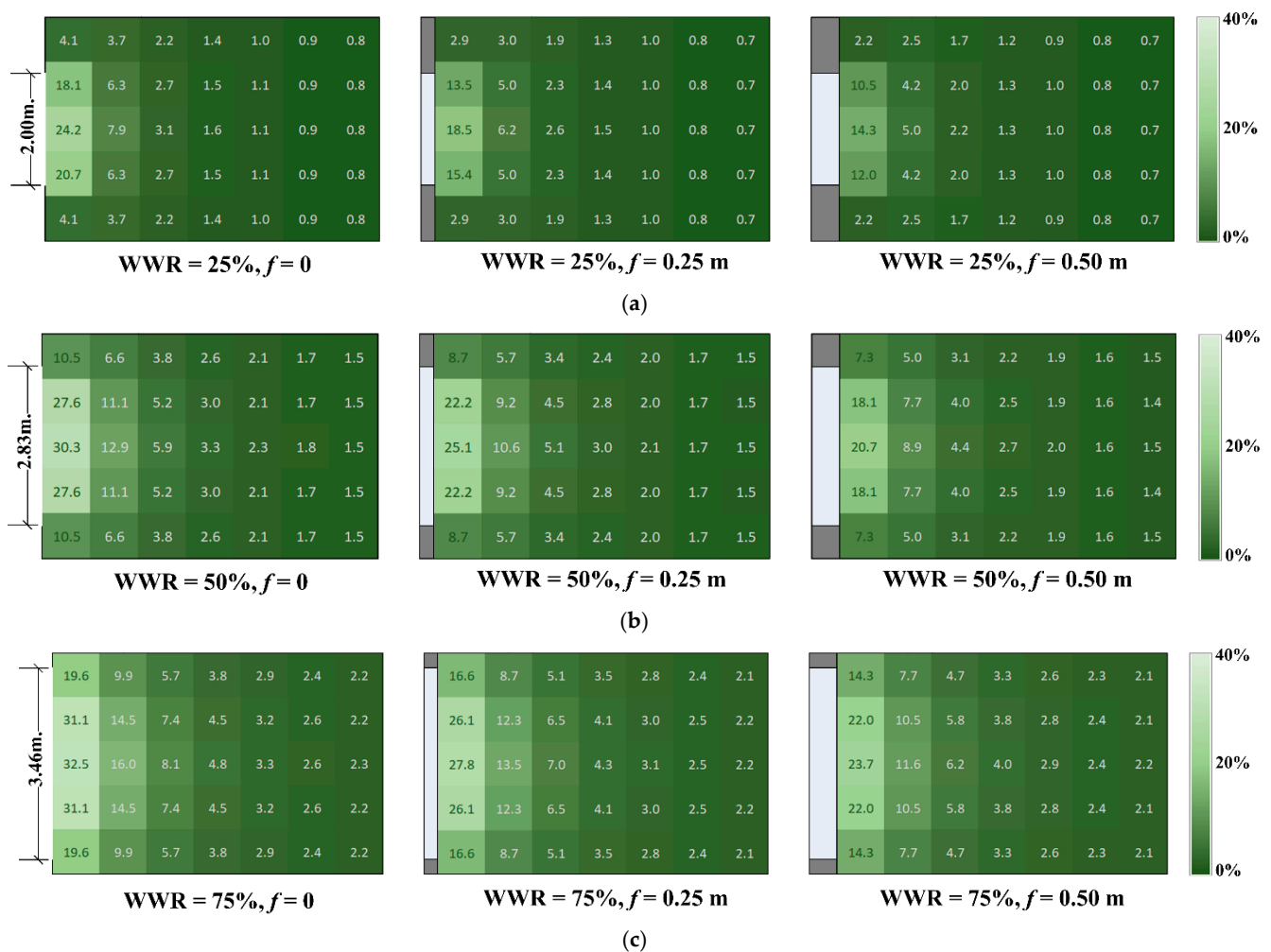


**Figure 11.** Spatial distribution plan of the DF on the workplane, at WWRs (a) 25%, (b) 50%, and (c) 75%, each for  $f = 0$ , 0.25, and 0.50 m.

It is observed that even under the standard CIE overcast sky, the spatial distribution of daylight within the room is very much uneven or non-uniform (cf. Figure 11), thus giving the qualitative ‘nuance’ of the space. For that reason, uniformity metrics are not considered in this study because they tend to ignore the fact that daylight distribution in a room is mostly uneven but is still appreciated. Thus, the worst-case scenario assumption does not necessarily mean that the qualitative aspect of daylight is ignored.

It is also noticed that regardless of the WWR and  $f$ , the DF values at the rear of the room are always maintained at 1–2%, as the values are largely influenced by the room surface reflectances, which are unchanged. The IRC model in Equation (18) is based on the principle of flux conservation, which is generally true for the given scenario.

Indeed, it is based on several assumptions, for instance, that the room surface reflectance is diffuse (Lambertian) and homogenous for the given area. It does not cover specific situations in which, for example, the surfaces have certain specularities, roughness, and non-homogeneity. However, in modelling and simulation practice, the assumption of diffuse and homogenous surface finishing areas is mostly acceptable and is sufficient to indicate the general tendency.

### 5.3. General Discussion

The goal of this study is to assess and quantify the theoretical impact of various façade thicknesses  $f$  on selected daylight metrics and annual lighting energy demand in a hypothetical reference office. While it can be anticipated that the impact on each metric will be different due to the different threshold or criterion, the numerical differences are yet to be provided in the literature, hence the motivation for this study. It is also understood that among all possible building design parameters, WWR plays a highly significant role in determining the outcome of the daylight calculation or simulation [13–45], so that the influence of  $f$  on the daylight metrics is presumably much less than the influence of WWR. Therefore, the analysis in this study only involves three distinct WWR values while involving 10 different  $f$  values, to focus on the effect of the latter rather than the former.

This study also finds that the WWR yields a greater impact on the daylight metrics compared to  $f$ . However, as mentioned in the Introduction, this study aims to assess the impact of  $f$  on those metrics, or to some extent, to prove the hypothesis that  $f$  has no influence on the metrics. The results suggest that several metrics, such as UDI-e and UDI-e', have a very small uncertainty due to varying  $f$  in scenes with a small opening area; but have large uncertainty in scenes with a large opening area. Meanwhile,  $DA_{300}$ ,  $sDA_{300/50\%}$ , and  $ED_{50\%}$  have the opposite behaviour. Thus, it can be argued that the findings of this study are non-trivial and can be obtained only after performing a systematic analysis.

A few remarks can be made regarding the presented results of this study. The results are bounded with the assumed room geometry and site location, even though the concept can still be applied in any location, provided the annual profile of outdoor diffuse daylight illuminance. In the reference [27], the WWR of the façade was set constant at 25%, following the generally recommended or optimum WWR values in the literature [13,14,35,45], between 20% and 30%. While assuming a value within that specific range may be reasonable, the observed effect of a façade thickness cannot be generalised, particularly for scenarios with a larger opening area. In the current study, situations with a larger WWR are also considered to provide more insights on the matter. Due to the use of the standard CIE overcast sky, however, the effect of building orientation is irrelevant in this study, as opposed to the earlier one that assumed the Perez sky model.

The absolute values in the outdoor diffuse illuminance ( $E_{out}$ ) profile are taken from the long-term measurement data in Makassar, Indonesia [37,38]. The  $E_{out}$  value of 10,000 lx is, in fact, recommended as the reference for daylight calculations under the typical overcast sky in the Indonesian national standard [46], due to the high probability of exceeding this value ( $P_{ex} > 90\%$ ), as shown in Figure 4. Other national standards, for instance, the former BS 8206-2:2008 [29], also published typical  $E_{out}$  profiles for the relevant region, but the absolute values are obviously lower than those in Indonesia. Nevertheless, the concept of using overcast sky data to predict climate-based daylight metrics has been demonstrated and validated using test cell measurements elsewhere [36] for various geographical latitudes, though not necessarily based on the annual  $E_{out}$  profile.

While it is understood that actual measurement data under the real-world overcast sky may be different from the theoretical values under the standard CIE overcast sky, Acosta et al. [36] proposed the following guidelines to ensure acceptable settings for overcast sky validation. In short, the sky ratio should be greater than 0.85; the measured luminance at the four cardinal orientations should be close to each other within  $\pm 5\%$  difference; and the measured  $E_{out}$  at the sampled time should be close to  $7/9\pi L_z$  [28] within  $\pm 10\%$  difference, where  $L_z$  is the zenith luminance at the particular time [36].

Thus, the proposed concept can still be applicable in a real-world situation, provided the conditions are satisfied.

The assumption of the worst-case scenario, i.e., under the standard CIE overcast sky, throughout this study is not a misleading attempt because the necessary conditions are all given in the first place. The results are also in agreement with the reference that employed annual simulation with weather data of similar locations in the tropics. Moreover, as mentioned in Section 3.1, there are 35 calculation points equally spaced on the workplane, and calculations are performed for all those points, not only on a single point. For simplicity, only metrics at the central calculation point and spatial metrics for the entire room are reported in Section 4. However, to obtain the spatial metrics, one obviously first needs to calculate the metric values at each calculation point; thus, no points are deliberately isolated. The plot across the façade thickness, if found linear, as in the case for the DF at the central point, suggests that the findings are consistent.

Regarding the room geometry, while it is clearly taken from a typical geometry of reference office space [25,27,39], it does not necessarily mean that all office spaces are always cuboids. However, in modelling and simulation practice, such an assumption is mostly acceptable and is sufficient to indicate the general tendency. In diagnostic tests, such as the CIE test cases [46,47] and BESTEST [48,49], the use of a cuboid room is also common, mostly because it serves the purpose. For other geometries, the results would certainly be different, but the concept can still be applied.

Moreover, in a realistic office space, the use of shading devices is indeed important in controlling direct sunlight penetration and the associated glare risk. However, this study focuses on the parametric effect of façade thickness, so that façade features other than the thickness itself and (selected values of) WWR are not considered. This is not to ignore the importance of shading devices in reality, but simply to focus the analysis on the defined input variables so that one can focus on them without intervention from other variables. Again, this is also a common practice in diagnostic tests, such as CIE test cases [46,47], in which shading devices are not present in the model, except when the test case is specifically conducted to observe the impact of such devices.

As described in Section 4.1, most of the plots between the metrics and the façade thickness in Figure 8 are more fluctuating and less 'linear' than the corresponding plots in Figure 7 because Figure 8 represents the spatial metrics. An exception is found for the  $DF_{av}$ , whose plot is also relatively linear, as in the case of the DF at the central point. The linearity of the  $DF_{av}$  plot is also confirmed in the simulation results of the earlier study [27], due to the relatively similar behaviour of the DF values at all calculation points that contribute to the  $DF_{av}$ .

Meanwhile, the unique pattern of UDI-a at the central point (Figure 7c), which has different directions (negative or positive) and gradients at different WWR, can only be observed when scenarios with large WWR values are considered. This was not performed in the earlier study; thus, a new insight is offered on this matter. From the sensitivity analysis results, it can be said that the trends for spatial metrics for the entire room are not necessarily similar to those at the central point. Different results can be expected if the single calculation point is located, for instance, at  $1/4$  or  $3/4$  of the room depth [14], or  $1/3$  of the room depth [50], or at the distance of 2 or 2.5 times the window-head height as per the well-known rule of thumb [51,52].

In general, finding the position of a single point that can best represent the spatial characteristics of daylight metrics in any given room is still an open yet relevant question because once known, one can save time and energy during in situ daylighting measurements by focusing on the representative point. This topic would be a follow-up to this research theme. Overall, the contribution of this study is providing insight into the impact of façade thickness on the sensitivity and uncertainty of various daylight metrics in indoor spaces. While no real experiments are involved in this study, the inter-model comparison with annual simulations using real weather data has been performed, and the results are generally in agreement. The concept is expected to be applicable in the case of site locations

where only the outdoor daylight diffuse illuminance profile is available or in the worst-case scenario under the standard CIE overcast sky.

## 6. Conclusions

Analytical daylighting calculations have been performed to predict the theoretical impact of non-zero façade thickness  $f$  ( $0 < f \leq 0.50$  m) on various daylight metrics and annual lighting energy demand in a reference office room under the standard CIE overcast sky, taking the case of the annual daylighting profile of a tropical city in Indonesia. Sensitivity analysis suggests that the variation of  $f$  yields different impacts on the observed metrics. The metrics DF,  $DA_{300}$ , and UDI- $a'$  are more sensitive to  $f$  in scenes with a small opening area. In those scenes, the UDI-e and UDI- $e'$  values are irrelevant because the upper threshold illuminance is never exceeded.

Among all metrics in the central calculation point,  $DA_{300}$ , UDI-a, and UDI- $a'$  yield relatively small coefficients of variation (CV), and thus, have the lowest uncertainty with respect to  $f$ . The greatest CV values (0.58) are found for UDI- $e'$ , particularly in scenes with a large opening area. Among all metrics for the entire room,  $sDA_{300/50\%}$  and  $sUDI-a_{50\%}$  have the lowest uncertainty, with an interquartile range of no more than 0.4%. Furthermore, several metrics, such as UDI-e and UDI- $e'$ , have a very small uncertainty in scenes with a small opening area; but have large uncertainty in scenes with a large opening area. Meanwhile,  $DA_{300}$ ,  $sDA_{300/50\%}$ , and  $ED_{50\%}$  have the opposite behaviour due to the defined illuminance threshold. In closure, this study has provided an insight on the impact of  $f$  on the sensitivity and uncertainty of various daylight metrics in indoor spaces, particularly in the worst-case scenario where the standard CIE overcast sky is applicable.

**Author Contributions:** Conceptualization, R.A.M.; methodology, R.A.M., Atthallah; software, R.A.M.; validation, R.A.M.; formal analysis, R.A.M.; investigation, R.A.M., Atthallah; resources, R.A.M.; data curation, R.A.M., Atthallah; writing—original draft preparation, R.A.M., Atthallah; writing—review and editing, R.A.M., Atthallah, M.D.K., B.Y.; visualization, R.A.M., Atthallah; supervision, M.D.K., B.Y.; project administration, R.A.M.; funding acquisition, R.A.M. All authors have read and agreed to the published version of the manuscript.

**Funding:** This research was funded by the Institute of Research and Community Services (LPPM) of Institut Teknologi Bandung (ITB), through the PPMI 2021 Research Program.

**Institutional Review Board Statement:** Not applicable.

**Informed Consent Statement:** Not applicable.

**Data Availability Statement:** The data presented in this study are available on request to the corresponding author.

**Conflicts of Interest:** The authors declare no conflict of interest.

## References

1. Bluysen, P.M.; Aries, M.; van Dommelen, P. Comfort of Workers in Office Buildings: The European HOPE Project. *Build. Environ.* **2011**, *46*, 280–288. [[CrossRef](#)]
2. Aries, M.B.C.; Veitch, J.A.; Newsham, G.R. Windows, View, and Office Characteristics Predict Physical and Psychological Discomfort. *J. Environ. Psychol.* **2010**, *30*, 533–541. [[CrossRef](#)]
3. Aries, M.B.C.; Aarts, M.P.J.; van Hoof, J. Daylight and Health: A Review of the Evidence and Consequences for the Built Environment. *Lighting Res. Technol.* **2015**, *47*, 6–27. [[CrossRef](#)]
4. Alzoubi, H.; Al-Rqaibat, S.; Bataineh, R.F. Pre-versus Post-Occupancy Evaluation of Daylight Quality in Hospitals. *Build. Environ.* **2010**, *45*, 2652–2665. [[CrossRef](#)]
5. Lim, G.-H.; Hirning, M.B.; Keumala, N.; Ghafar, N.A. Daylight Performance and Users' Visual Appraisal for Green Building Offices in Malaysia. *Energy Build.* **2017**, *141*, 175–185. [[CrossRef](#)]
6. Jamrozik, A.; Clements, N.; Hasan, S.S.; Zhao, J.; Zhang, R.; Campanella, C.; Loftness, V.; Porter, P.; Ly, S.; Wang, S.; et al. Access to Daylight and View in an Office Improves Cognitive Performance and Satisfaction and Reduces Eye Strain: A Controlled Crossover Study. *Build. Environ.* **2019**, *165*, 106379. [[CrossRef](#)]
7. Davoodi, A.; Johansson, P.; Henricson, M.; Aries, M. A Conceptual Framework for Integration of Evidence-Based Design with Lighting Simulation Tools. *Buildings* **2017**, *7*, 82. [[CrossRef](#)]

8. Hirning, M.B.; Isoardi, G.L.; Coyne, S.; Garcia Hansen, V.R.; Cowling, I. Post Occupancy Evaluations Relating to Discomfort Glare: A Study of Green Buildings in Brisbane. *Build. Environ.* **2013**, *59*, 349–357. [[CrossRef](#)]
9. Hirning, M.B.; Isoardi, G.L.; Cowling, I. Discomfort Glare in Open Plan Green Buildings. *Energy Build.* **2014**, *70*, 427–440. [[CrossRef](#)]
10. Handina, A.; Mukarromah, N.; Mangkuto, R.A.; Atmodipoero, R.T. Prediction of Daylight Availability in a Large Hall with Multiple Facades Using Computer Simulation and Subjective Perception. *Procedia Eng.* **2017**, *170*, 313–319. [[CrossRef](#)]
11. Goia, F.; Haase, M.; Perino, M. Optimizing the Configuration of a Façade Module for Office Buildings by Means of Integrated Thermal and Lighting Simulations in a Total Energy Perspective. *Appl. Energy* **2013**, *108*, 515–527. [[CrossRef](#)]
12. Zhang, A.; Bokel, R.; van den Dobbelsteen, A.; Sun, Y.; Huang, Q.; Zhang, Q. Optimization of Thermal and Daylight Performance of School Buildings Based on a Multi-Objective Genetic Algorithm in the Cold Climate of China. *Energy Build.* **2017**, *139*, 371–384. [[CrossRef](#)]
13. Ghisi, E.; Tinker, J.A. An Ideal Window Area Concept for Energy Efficient Integration of Daylight and Artificial Light in Buildings. *Build. Environ.* **2005**, *40*, 51–61. [[CrossRef](#)]
14. Ochoa, C.E.; Aries, M.B.C.; van Loenen, E.J.; Hensen, J.L.M. Considerations on Design Optimization Criteria for Windows Providing Low Energy Consumption and High Visual Comfort. *Appl. Energy* **2012**, *95*, 238–245. [[CrossRef](#)]
15. González, J.; Fiorito, F. Daylight Design of Office Buildings: Optimisation of External Solar Shadings by Using Combined Simulation Methods. *Buildings* **2015**, *5*, 560–580. [[CrossRef](#)]
16. Acosta, I.; Campano, M.Á.; Molina, J.F. Window Design in Architecture: Analysis of Energy Savings for Lighting and Visual Comfort in Residential Spaces. *Appl. Energy* **2016**, *168*, 493–506. [[CrossRef](#)]
17. Mangkuto, R.A.; Rohmah, M.; Asri, A.D. Design Optimisation for Window Size, Orientation, and Wall Reflectance with Regard to Various Daylight Metrics and Lighting Energy Demand: A Case Study of Buildings in the Tropics. *Appl. Energy* **2016**, *164*, 211–219. [[CrossRef](#)]
18. Özel, G.; Açikkalp, E.; Görgün, B.; Yamık, H.; Caner, N. Optimum Insulation Thickness Determination Using the Environmental and Life Cycle Cost Analyses Based Entransy Approach. *Sustain. Energy Technol. Assess.* **2015**, *11*, 87–91. [[CrossRef](#)]
19. Olivieri, F.; Grifoni, R.C.; Redondas, D.; Sánchez-Reséndiz, J.A.; Tascini, S. An Experimental Method to Quantitatively Analyse the Effect of Thermal Insulation Thickness on the Summer Performance of a Vertical Green Wall. *Energy Build.* **2017**, *150*, 132–148. [[CrossRef](#)]
20. Braulio-Gonzalo, M.; Bovea, M.D. Environmental and Cost Performance of Building’s Envelope Insulation Materials to Reduce Energy Demand: Thickness Optimisation. *Energy Build.* **2017**, *150*, 527–545. [[CrossRef](#)]
21. Barrau, J.; Ibañez, M.; Badia, F. Impact of the Optimization Criteria on the Determination of the Insulation Thickness. *Energy Build.* **2014**, *76*, 459–469. [[CrossRef](#)]
22. Azari, R.; Garshashi, S.; Amini, P.; Rashed-Ali, H.; Mohammadi, Y. Multi-Objective Optimization of Building Envelope Design for Life Cycle Environmental Performance. *Energy Build.* **2016**, *126*, 524–534. [[CrossRef](#)]
23. Ashouri, M.; Astaraei, F.R.; Ghasempour, R.; Ahmadi, M.H.; Feidt, M. Optimum Insulation Thickness Determination of a Building Wall Using Exergetic Life Cycle Assessment. *Appl. Therm. Eng.* **2016**, *106*, 307–315. [[CrossRef](#)]
24. Zhou, B.; Yoshioka, H.; Noguchi, T.; Ando, T. Effects of Opening Edge Treatment and EPS Thickness on EPS External Thermal Insulation Composite Systems (ETICS) Façade Reaction-to-Fire Performance Based on JIS A1310 Standard Façade Fire Test Method. *Fire Mater.* **2018**, *42*, 537–548. [[CrossRef](#)]
25. Van Dijk, D.; Platzer, W. *Reference Office for Thermal, Solar and Lighting Calculations, Report No. Swift-Wp3-Tno-Dvd-030416. International Energy Agency (IEA) Task 27; TNO Building and Construction Research: Delft, The Netherlands; Fraunhofer Institute for Solar Energy Systems: Freiburg, Germany, 2003.*
26. Reinhart, C.F.; Jakubiec, J.; Ibarra, D. Definition of a Reference Office for Standardized Evaluations of Dynamic Façade and Lighting Technologies. In Proceedings of the Building Simulation 2013—13th Conference of International Building Performance Simulation Association, Chambéry, France, 26–28 August 2013.
27. Mangkuto, R.A.; Fela, R.F.; Utami, S.S. Effect of Façade Thickness on Daylight Performance in a Reference Office Building. In Proceedings of the Building Simulation 2019—16th Conference of International Building Performance Simulation Association, Rome, Italy, 2–4 September 2019.
28. Moon, P.; Spencer, D.E. Illumination from a Non-Uniform Sky. *Trans. Illum. Eng. Soc.* **1942**, *37*, 707–726.
29. British Standard Institution (BSI). *BS 8206-2:2008: Lighting for Buildings—Part 2: Code of Practice for Daylighting*; British Standard Institution: London, UK, 2008.
30. Comité Européen de Normalisation (CEN). *EN 17037:2018: Daylight in Buildings*; Comité Européen de Normalisation: Brussels, Belgium, 2018.
31. Seshadri, T.N. Equations of Sky Components with a “C.I.E. Standard Overcast Sky”. *Proc. Indian Acad. Sci.* **1960**, *51*, 233–242. [[CrossRef](#)]
32. Hopkinson, R.G.; Petherbridge, P.; Longmore, J. *Daylighting*; Heinemann: London, UK, 1966.
33. Andersen, M. Generalization of the Direct Sky Component Calculation to Openings of Arbitrary Tilt Angle. *LEUKOS* **2005**, *1*, 39–55. [[CrossRef](#)]
34. Tregenza, P.R. Modification of the Split-Flux Formulae for Mean Daylight Factor and Internal Reflected Component with Large External Obstructions. *Lighting Res. Technol.* **1989**, *21*, 125–128. [[CrossRef](#)]

35. Szokolay, S.V. *Introduction to Architectural Science: The Basis of Sustainable Design*, 2nd ed.; Architectural Press: Oxford, UK, 2008; ISBN 978-0-7506-8704-1.
36. Acosta, I.; Campano, M.Á.; Domínguez, S.; Fernández-Agüera, J. Minimum Daylight Autonomy: A New Concept to Link Daylight Dynamic Metrics with Daylight Factors. *LEUKOS* **2019**, *15*, 251–269. [[CrossRef](#)]
37. Rahim, R. *Teori Dan Aplikasi Distribusi Luminansi Langit Di Indonesia [Theory and Application of Sky Luminance Distribution in Indonesia]*; Universitas Hasanuddin: Makassar, Indonesia, 2009. (In Indonesian)
38. Rahim, R.; Baharuddin; Mulyadi, R. Classification of Daylight and Radiation Data into Three Sky Conditions by Cloud Ratio and Sunshine Duration. *Energy Build.* **2004**, *36*, 660–666. [[CrossRef](#)]
39. Mangkuto, R.A.; Siregar, M.A.A.; Handina, A.; Faridah. Determination of Appropriate Metrics for Indicating Indoor Daylight Availability and Lighting Energy Demand Using Genetic Algorithm. *Sol. Energy* **2018**, *170*, 1074–1086. [[CrossRef](#)]
40. United States Green Building Council (USGBC). *LEED v4.1: Building Design and Construction*; USGBC Inc.: Washington, DC, USA, 2021.
41. Nabil, A.; Mardaljevic, J. Useful Daylight Illuminances: A Replacement for Daylight Factors. *Energy Build.* **2006**, *38*, 905–913. [[CrossRef](#)]
42. Mardaljevic, J.; Andersen, M.; Roy, N.; Christoffersen, J. Daylighting Metrics: Is There a Relation between Useful Daylight Illuminance and Daylight Glare Probability? In Proceedings of the Building Simulation and Optimization Conference 2012, Loughborough, UK, 10–11 September 2012; pp. 189–196.
43. Gan, W.; Cao, Y.; Jiang, W.; Li, L.; Li, X. Energy-Saving Design of Building Envelope Based on Multiparameter Optimization. *Math. Probl. Eng.* **2019**, *2019*, 5261869. [[CrossRef](#)]
44. Chan, A. *Methods for Daylight Factor Estimation*; City University of Hong Kong: Kowloon Tong, Hongkong, 2008.
45. Mangkuto, R.A.; Asri, A.D.; Rohmah, M.; Soelami, F.X.; Soegijanto, R.M. Revisiting the National Standard of Daylighting in Indonesia: A Study of Five Daylit Spaces in Bandung. *Sol. Energy* **2016**, *126*, 276–290. [[CrossRef](#)]
46. Commission Internationale de l'Éclairage (CIE). *CIE 171:2006—Test Cases to Assess the Accuracy of Lighting Computer Program*; CIE: Vienna, Austria, 2006.
47. Maamari, F.; Fontoynt, M.; Adra, N. Application of the CIE test cases to assess the accuracy of lighting computer programs. *Energy Build.* **2006**, *38*, 869–877. [[CrossRef](#)]
48. Judkoff, R.; Neymark, J. *International Energy Agency Building Energy Simulation Test (BESTEST) and Diagnostic Method*; Report NREL/TP-472-6231; NREL: Golden, CO, USA, 1995.
49. American Society of Heating, Refrigerating, and Air Conditioning (ASHRAE). *ANSI/ASHRAE Standard 140-2004: Standard Method of Test for the Evaluation of Building Energy Analysis Computer Programs*; ASHRAE: Atlanta, GA, USA, 2004.
50. Badan Standardisasi Nasional (BSN). *SNI 03-2396-2001: Tata Cara Perancangan Sistem Pencahayaannya Alami Pada Bangunan Gedung. [Design Guidelines for Daylighting System in Buildings]*; Badan Standardisasi Nasional (BSN): Jakarta, Indonesia, 2001. (In Indonesian)
51. Reinhart, C.F. A Simulation-Based Review of the Ubiquitous Window-Head-Height to Daylit Zone Depth Rule of Thumb. In Proceedings of the Building Simulation 2005—9th Conference of International Building Performance Simulation Association, Montreal, QC, Canada, 15–18 August 2000.
52. Reinhart, C.F.; Weissman, D.A. The Daylit Area—Correlating Architectural Student Assessments with Current and Emerging Daylight Availability Metrics. *Build. Environ.* **2012**, *50*, 155–164. [[CrossRef](#)]